



Rivers and tidal flats as sources of dissolved organic matter and trace metals in the German Bight (North Sea)

Linn G. Speidel · Roger Carvalho da Silva · Melanie Beck ·
Olaf Dellwig · Jochen Wollschläger · Thorsten Dittmar ·
Michael Seidel

Received: 20 December 2022 / Accepted: 2 January 2024 / Published online: 9 March 2024
© The Author(s) 2024

Abstract The German Bight in the southern North Sea receives nutrients, dissolved organic matter (DOM), and trace metals from rivers, porewater reflux, and porewater outwelling. We studied the marine, riverine, and porewater sources analyzing molecular transformations of solid-phase extracted (SPE) DOM in the German Bight. We applied a combination of ultrahigh-resolution mass spectrometry (FT-ICR-MS) with quantitative data of dissolved organic sulfur (DOS), dissolved black carbon (DBC), dissolved trace metals (Ba, Co, Gd, Mo, Mn, W), and nutrients (nitrite, nitrate, phosphate, silicate). While aromatic DOM and DBC mainly originated from the

rivers, nitrogen-containing, more saturated DOM was enriched offshore suggesting greater contributions of marine (algal) sources. Except for dissolved Mo, rivers were the primary source of trace metals and nutrients. However, tidal flats contributed to dissolved nutrient (e.g., dissolved phosphate), trace metal and DOS inventories of the southern North Sea. The input of DOS from intertidal flats was identified by the molecular index derived from sulfidic porewaters (I_{SuP}), non-conservative behavior of elemental sulfur-to-carbon ratio and sulfur content of molecular formulae (from FT-ICR-MS). Dissolved Mn and Si were removed in the German Bight, likely due to precipitation as Mn(hydr)oxides and biological uptake, respectively. Preliminary estimates suggest that DOS from porewater outwelling is approximately four times higher than DOS discharged by the three main rivers in the region. Our study therefore highlights the need to consider porewater discharge in addition to riverine sources to comprehensively assess elemental budgets within the complex interplay and

Responsible Editor: Francis Chan.

Linn G. Speidel and Roger Carvalho da Silva have contributed equally to this work and share first authorship.

Supplementary Information The online version contains supplementary material available at <https://doi.org/10.1007/s10533-024-01117-3>.

L. G. Speidel · R. Carvalho da Silva · M. Beck ·
J. Wollschläger · T. Dittmar · M. Seidel (✉)
Institute for Chemistry and Biology of the Marine
Environment (ICBM), Carl von Ossietzky Universität
Oldenburg, 26129 Oldenburg, Germany
e-mail: m.seidel@uni-oldenburg.de

Present Address:

L. G. Speidel
Department of Earth Sciences, ETH Zurich, 8092 Zurich,
Switzerland

O. Dellwig
Leibniz Institute for Baltic Sea Research Warnemünde
(IOW), 18119 Rostock, Germany

T. Dittmar
Helmholtz Institute for Functional Marine Biodiversity
at Carl von Ossietzky Universität Oldenburg (HIFMB),
26129 Oldenburg, Germany

transformations of DOM, nutrients, and trace metals in coastal ecosystems.

Keywords Ultrahigh-resolution mass spectrometry · Dissolved organic matter · Dissolved black carbon · Dissolved organic sulfur · Trace metals · Estuaries · Tidal cycle

Introduction

Land–ocean interfaces play a key role in controlling fluxes of dissolved organic matter (DOM), nutrients and trace metals in global biogeochemical cycles (Burnett et al. 2003; Moore et al. 2006; Canuel et al. 2012). Yet, carbon dynamics and their connection to nutrients and trace metals in coastal ecosystems are still not fully understood, limiting our ability to accurately quantify global carbon fluxes (Ward et al. 2017).

Coastal ecosystems and estuaries are hotspots for DOM cycling (Tzortziou et al. 2008). Estuarine DOM originates from allochthonous (marine, riverine, groundwater, and atmospheric input) and autochthonous sources (in situ production) (Osterholz et al. 2016; Riedel et al. 2016). The DOM composition in estuaries and coastal ecosystems is influenced by exchanges with intertidal systems (Letourneau et al. 2021), atmospheric deposition and microbial transformations (Carey and Fulweiler 2014; Tzortziou et al. 2008). Primary production in coastal environments is enhanced by the riverine supply of nutrients. This, together with estuarine DOM sources and transformations, make DOM dynamics in coastal environments extremely complex (Yamashita, et al. 2008). Not only large rivers have an influence on the biogeochemistry of coastal environments (Medeiros et al. 2015b) but also small coastal tributaries (Beck et al. 2012), intertidal beaches (Beck et al. 2017; Santos et al. 2008; Seidel, et al. 2015a), and intertidal flats such as in the Wadden Sea of the southern North Sea (Beck and Brumsack 2012; Reckhardt et al. 2015; Seidel et al. 2014). In all these systems, biogeochemical cycles are largely influenced by porewater outwelling, i.e., lateral fluxes or horizontal exports, including submarine groundwater discharge (SGD) and advective transport across the water–sediment interface (Beck et al. 2008b; Moore et al. 2011; Santos et al. 2021a, 2015). Because of higher porewater concentrations

of dissolved organic carbon (DOC), inorganic nutrients, and certain trace metals compared to river water, porewater outwelling is a major factor regulating their fluxes in coastal areas (Beck et al. 2008a; Grunwald et al. 2010; Moore et al. 2011; Reckhardt et al. 2015).

Oceanic DOM contains one of the largest active organic carbon pools on earth (Hansell 2013) and is mostly derived from marine primary producers such as phytoplankton (Carlson and Hansell 2015). However, terrestrial DOM input by rivers and porewater outwelling is important in coastal oceans (Santos et al. 2021b, 2021a; Ward et al. 2017). DOM is a highly complex mixture that is still not fully characterized (Dittmar and Stubbins 2014; Koch et al. 2005; Nebbioso and Piccolo 2013). With ultrahigh-resolution Fourier-transform ion cyclotron resonance mass spectrometry (FT-ICR-MS) it is, however, possible to determine thousands of molecular formulae in the complex DOM mixture (Zark and Dittmar 2018). FT-ICR-MS thus has become an important tool to study the DOM molecular composition in ecosystems ranging from the oceanic water column (Gonsior et al. 2011; Hansman et al. 2015; Medeiros et al. 2015a), through estuaries (Medeiros et al. 2015b; Osterholz et al. 2016), to porewater (Schmidt et al. 2009; Seidel et al. 2014). The DOM molecular composition carries valuable information of its sources and processing such as photo- and bio-transformations (Medeiros et al. 2015b; Stubbins et al. 2012).

Marine DOM contains dissolved black carbon (DBC) that is mainly generated through the incomplete combustion of organic matter on land, consisting of polycyclic and condensed aromatics (Wagner et al. 2018). Non-pyrogenic sources are, for example, petroleum-derived (Podgorski et al. 2021; Brünjes et al. 2022) as well as fungal compounds (Brodowski et al. 2005). In fire-impacted catchments like in our study, charring and soot deposition are, however, quantitatively by far the most important sources of black carbon (Brodowski et al. 2005; Coppola et al. 2022). Overall, the ocean stores about 14 Pg of DBC (Coppola et al. 2022), representing a carbon fraction that persists for several millennia due to its recalcitrance (Coppola and Druffel 2016). Rivers and atmospheric deposition are major transport pathways of DBC from land to the ocean (Bao et al. 2017; Jaffé et al. 2013), whereas porewater sources remain poorly understood. Photo-degradation is a major sink for recalcitrant DBC in the surface ocean (Dittmar and

Paeng 2009; Stubbins et al. 2012) and DBC removal is enhanced in clear offshore waters where photochemical reactions are the dominant pathway for DOM transformations compared to more turbid river plumes and coastal waters (Medeiros et al. 2015b).

Marine DOM contains about 7 Pg dissolved organic sulfur (DOS) (Ksionzek et al. 2016; Longnecker et al. 2020). It is mainly derived from marine primary production (Phillips et al. 2022) but abiotic sulfurization of DOM (Pohlabeln et al. 2017) is a considerable DOS source in sulfidic sediments (Seidel et al. 2014). Such addition of sulfur may protect organic matter from microbial alteration (Anderson and Pratt 1995), also determining mobility and bioavailability of trace metals (Marie et al. 2015). Most marine DOS appears to be part of active biogeochemical cycling (Ksionzek et al. 2016; Phillips et al. 2022), but a fraction of porewater-derived DOS is distributed globally and reaches the deep ocean as part of the refractory DOM (Phillips et al. 2022). However, riverine and porewater sources of DOS in coastal oceans are not well constrained yet.

In aquatic environments, redox-sensitive trace metals exist in soluble and particulate form, depending on factors such as pH, salinity, redox-condition, productivity, DOM, and suspended matter (Chester and Jickells 2012). Sources include rivers, groundwater, and porewater reflux, dust or aerosols (Bruland and Lohan 2003). Trace metal removal is controlled by biological uptake, scavenging onto particles, availability of ligands, and redox gradients (Bruland and Lohan 2003). Thus, studying redox-sensitive trace metals in the context of (dissolved) organic matter helps understanding redox characteristics of the depositional and diagenetic environments and DOM cycling (Miller et al. 2011; Morford et al. 2007; Mori et al. 2019; Tribovillard et al. 2006).

In detail, manganese (Mn) and iron (Fe) (oxyhydr-) oxides scavenge DOM and trace metals (Berrang and Grill 1974; Bruland and Lohan 2003; Burdige 1993; Linkhorst et al. 2017), and co-precipitation with Fe oxide minerals traps significant portions of DBC at sediment–water redox-interface (Riedel et al. 2013) as well as nutrients such as phosphate (e.g. Slomp et al. 1996). Manganese and Fe are delivered to the southern North Sea by rivers (Beck et al. 2020; Laxen et al. 1984; Vuori 1995) and porewater outwelling from oxygen-deficient intertidal systems (Beck et al. 2008b; Dellwig et al. 2007a, b; Moore et al. 2011;

Mori et al. 2019). The studied trace metals Cobalt (Co), molybdenum (Mo), tungsten (W), barium (Ba), and gadolinium (Gd) do not directly influence DOM concentrations or characteristics, but they are helpful tools to decipher environmental conditions and sources. Molybdenum generally behaves conservatively in the open ocean (Collier 1985; Morris 1975). However, non-conservative behavior in coastal settings such as the southern North Sea was related to phytoplankton blooms and possibly to scavenging in oxygen-deficient micro-niches of suspended particles (Dellwig et al. 2007a; Kowalski et al. 2013). Comparable to Mo, tungsten (W) behaves conservatively in the oxygenated ocean (Firdaus et al. 2008; Sohrin et al. 1999) but appears at a magnitudes lower concentration than Mo, most likely due to a lowered susceptibility to weathering, a lower solubility and a higher affinity to Fe–Mn oxyhydroxides representing the dominating oceanic sink of W (Dellwig et al. 2019; Kashiwabara et al. 2017). Dissolved barium (Ba) is used in coastal ocean studies as a tracer for porewater outwelling because it shares geochemical similarities with porewater tracers such as radium (Gonneea et al. 2013) and is released from intertidal sediments (Moore 1997; Mori et al. 2019; Seidel et al. 2014). Similarly, Mn, Co, and W are enriched in oxygen-depleted or sulfidic porewater and are released to the open water column by porewater outwelling (Cui et al. 2021; Dellwig et al. 2019, 2021; Mohajerin et al. 2016). Gadolinium is a specific tracer for anthropogenic input due to the usage of organic Gd complexes as contrast agents in magnetic resonance imaging (Kulaksiz and Bau 2007; Rogowska et al. 2018) leading to positive anomalies in rivers (Kulaksiz and Bau 2007), terrestrial groundwater (Johannesson et al. 2017), and coastal waters (Hatje et al. 2016; Pedreira et al. 2018).

Previous studies have demonstrated the importance of intertidal flats and rivers as drivers of nutrient, carbon (e.g. methane and chromophoric DOM) and trace metal dynamics in the North Sea (e.g. Beck and Brumsack 2012; Grunwald et al. 2010, 2009; Kowalski et al. 2009; Lübben et al. 2009; Moore et al. 2011; Painter et al. 2018). However, it remains a major challenge to decipher the different DOM sources, i.e., marine, estuarine, fluvial, and porewater in highly complex coastal settings such as the southern North Sea. Our study therefore aims to differentiate sources and sinks of DOM in the German Bight (southeastern

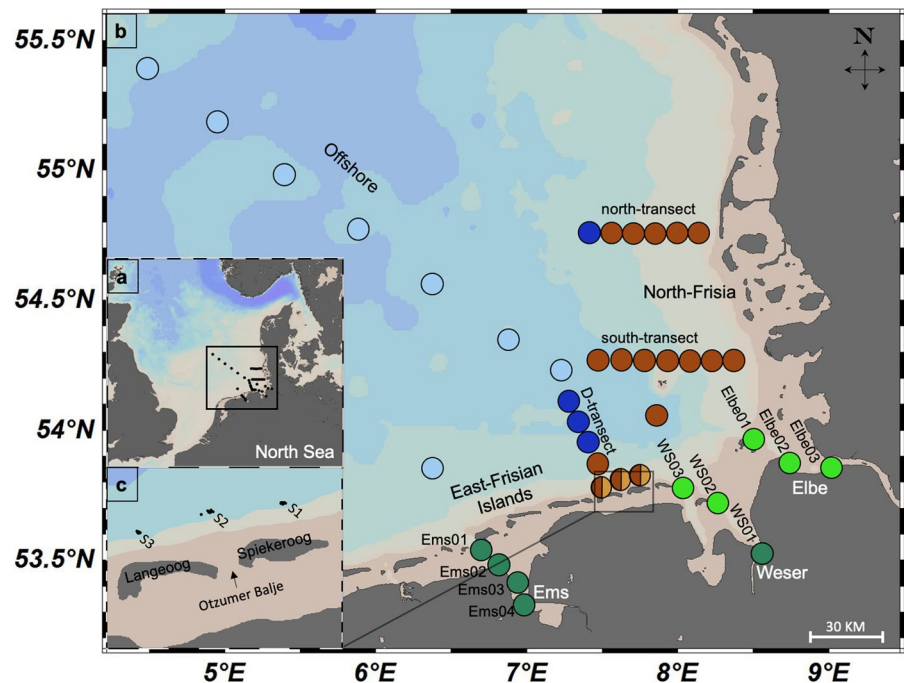
North Sea) from the three main estuaries (rivers Elbe, Weser, and Ems) and the intertidal flats. We hypothesize that sulfate-reducing intertidal sediments are hotspots of abiotic sulfurization of DOM, producing DOS that is carried via porewater outwelling into the coastal zone. We further hypothesize that, besides riverine input, porewater outwelling is a source of DBC due to the mobilization of previously deposited black carbon from intertidal sediments. In this context, we address how the molecular DOM composition is linked to the environmental and redox conditions at the formation sites as characterized by concentrations of chlorophyll *a*, dissolved oxygen (DO), dissolved trace metals (Ba, Co, Mn, Mo, W, and Gd), and pH values. In addition to nutrients (dissolved nitrogen species, phosphate, and silicate), dissolved trace metals such as Ba, Co or Mn can escape from intertidal sediments to the coastal ocean via porewater outwelling, and we hypothesize that the transport of the released trace metals and their potential precipitation further offshore are connected to the export of DOM to the German Bight.

Material and methods

Study site

The coastal area of the German Bight in the southeastern North Sea (Hofmann et al. 2005) covers the Islands and Wadden Sea of East and North Frisia (Fig. 1). The Wadden Sea, extending from Den Helder (Netherlands) to Esbjerg (Denmark), forms the largest uninterrupted stretch of sand and mudflats in the world (Marencic 2009). Water depths in the German Bight sector range between <10 m nearshore to >40 m offshore increasing in direction to the Atlantic Ocean to ~200 m (Becker et al. 1992; OSPAR 2000). Semidiurnal tides range between 2 to 4 m, with macro-tidal estuaries at the Elbe and Weser Rivers and meso-tidal coasts at East and North Frisia (Zeiler et al. 2008). Water masses originate from the Atlantic Ocean north of Scotland and through the English Channel, rivers such as Humber, Thames, Scheldt, Rhine, Ems, Weser, and Elbe (Becker et al. 1992), and finally outflow of brackish waters from the Baltic Sea (Painter et al. 2018). Main freshwater sources to the German Bight are the rivers Elbe, Weser, and Ems, but contributions also occur via smaller fluvial watercourses that drain the hinterland and are connected to the tidal flat areas by

Fig. 1 Map showing the German Bight in the southern North Sea (a) the coasts of North and East Frisia and the rivers Elbe, Weser, and Ems (b) and the stations of tidal cycle sampling (S1–S3) close to the islands of Spiekeroog and Langeoog and the tidal inlet Otzumer Balje (arrow), respectively (c). The color codes of the sampling stations refer to clusters that were determined by multivariate statistical analysis: River 1 (light green) and River 2 (dark green), Wadden Sea (light brown) and coastal transition (dark brown) as well as marine offshore 1 (light blue) and offshore 2 (dark blue) stations



flood-gates, depending on precipitation in the drainage area (Beck et al. 2012). The Elbe River is the largest freshwater source ($861 \text{ m}^3 \text{ s}^{-1}$) to the German Bight followed by the rivers Weser ($323 \text{ m}^3 \text{ s}^{-1}$) and Ems ($80 \text{ m}^3 \text{ s}^{-1}$) (Lübben et al. 2009; Schmidt et al. 2011 and references therein). Barrier islands separate the backbarrier tidal flat areas from the nearshore North Sea. Most of the barrier islands are separated by tidal inlets (< 5 to 15 m deep) such as the Otzumer Balje between the islands of Langeoog and Spiekeroog (Fig. 1c; Valle-Levinson et al. 2018). During low tide, the backbarrier tidal flats are exposed thereby discharging porewater into the tidal channels (Moore et al. 2011).

Sampling

Sampling in the German Bight and the estuaries was carried out from 19th to 31st March 2019 aboard *R/V Heincke* (leg HE527) (Supplementary Table S1), at the onset of the phytoplankton bloom but before the main phytoplankton bloom (around April). A total number of 78 water column samples were collected at 71 stations along transects close to the East- and North-Frisian Islands, in the offshore part of the German Bight and in the Ems, Weser and Elbe estuaries (Fig. 1; Supplementary Table S1). Tidal cycles were sampled at three stations over ~ 50 h, with a time interval of 1.5 h, off the islands of Langeoog and Spiekeroog close to the tidal inlet Otzumer Balje (Fig. 1c). Samples were taken with a rosette water sampler equipped with twelve Niskin bottles and a CTD (conductivity, temperature, pressure). Samples were taken in acid-rinsed pH 2 (HCl 25%, p.a.) 20 L HDPE carboys, filtered with a Masterflex peristaltic pump using a Causa pure pre-filter cartridge (CPR-001-09-DOX, 1 μm , 10-inch, PP, Infiltec) and a Causa-PES filter cartridge (CPS-S10-10-DOV-A, 0.1 μm , 10-inch, PES, Infiltec), in Causa PP blue filter holders (PBD-10-GFE, 10 inches, Infiltec) connected via Masterflex Chem-durance tubing. After filtration, an aliquot was taken for the measurements of fluorescent DOM (FDOM). For DOM extraction, 1 L of filtered sample was acidified to pH 2 (HCl 25%, p.a.). Triplicates of filtered samples were taken in 30 mL HDPE bottles for DOC analysis. Samples for trace metal and nutrient analyses were filtered through 0.45 μm SFCA (surfactant-free cellulose acetate) syringe filters into polyethylene bottles (acid-washed and

rinsed with ultrapure water prior to usage for trace metal samples). Saturated mercury(II)chloride solution (HgCl_2) was added to the nutrient samples for preservation after Schnetger and Lehnert (2014). Trace metal samples were acidified using concentrated ultrapure HNO_3 to obtain a concentration of 1% (v/v). All trace metal samples were stored in the dark at 4°C and were measured within eight months, nutrient measurements were done within a week after sampling. The storage of fixed seawater samples over several months does not affect the stability of the trace metal inventory (Dellwig et al. 2019).

Bulk geochemical analyses

Humic-like FDOM was measured in filtered water samples (without acidification) using an AquaFluor handheld Fluorometer/Turbidimeter 8000-010 made by Turner Designs (excitation 350 nm, emission 450 nm) and results are given in relative fluorescence units (rfu). The handheld fluorometer semi-quantitatively targets humic-like fluorescence DOM (peak C) (Coble 1996; Waska et al. 2019). Dissolved organic carbon (DOC) and total dissolved nitrogen (TDN), which is the sum of nitrate (NO_3^-), nitrite (NO_2^-), ammonia (NH_4^+), and dissolved organic nitrogen (DON), were measured with the high temperature catalytic oxidation (HTCO) method on a DOC Analyzer (Shimadzu TOC-V_{CPH}) equipped with a TDN unit. Analytical precision and trueness were better than 5% (tested against deep-sea reference material provided by Dennis Hansell at the University of Miami, USA) and low-carbon ultrapure water. Solid-phase extraction (SPE) of DOM from 1 L water samples (adjusted to pH 2, HCl 25%, p.a.) was performed as described by Dittmar (2008) using styrene divinyl benzene polymer filled cartridges (Agilent Bond Elut PPL, 1g). After drying the cartridges, DOM was eluted with 6 mL methanol (HPLC grade). The SPE-DOM extracts were stored in brown glass vials at -20°C for further analyses. The extraction efficiency was calculated as DOC concentrations in original water samples compared to DOC concentrations in methanol extracts by drying an aliquot of the extract at 40°C and re-dissolving it in ultrapure water. The average extraction efficiency was $52.7 \pm 5.9\%$ of total DOC. Concentrations of dissolved inorganic phosphorus (DIP), dissolved silicate (DSi), nitrogen oxides (NO_x , which is the sum of NO_3^- and NO_2^-), and NO_2^- were analyzed

using a Multiscan GO Microplate Spectrophotometer (Thermo Scientific) and an EasyChem Plus discrete analyzer (AMS-SYSTE) after Schnetger and Lehnert (2014), Reckhardt et al. (2015), and Mori et al. (2021). Nitrate concentrations were calculated as the difference between NO_x and NO_2^- . Precision and trueness were verified using solutions containing defined concentrations of NO_x , NO_2^- , PO_4^{3-} , and DSI and were better than 10%.

Further oceanographic and biogeochemical parameters were measured continuously (1 min interval) in the surface water using a FerryBox system (Petersen et al. 2003). The water intake of the systems was in the moon pool of the ship at ~4 m depth. The FerryBox contained sensors for salinity and temperature (Teledyne Citadel), chlorophyll *a* (Chl *a*) fluorescence (SCUFA, Turner Designs), DO (optode, Aanderaa), and a pH-electrode (Meinsberg). The pH-electrode was calibrated before the cruise using three different standard solutions (pH 5, 7, and 9, respectively). The salinity and temperature sensor as well as the oxygen optode were used with their manufacturer calibrations. Fluorescence readings of Chl *a* were converted into Chl *a* concentration using discrete sample data (R^2 of the linear correlation: 0.67). For these data, water samples from ~4 m depth were collected with a rosette water sampler equipped with Niskin bottles. A water volume of 0.2 to 6.5 L (depending on concentration of particulate matter) was filtered through GF/F filters (0.7 μm pore size), which were frozen immediately at -80°C until laboratory analysis. Pigments were extracted within 6 months after the cruise by incubating the filters in 90% acetone–water solution overnight at 4°C . Additionally, empty filters were extracted as blanks. Extracts were centrifuged for 10 min at $3,020\times g$ and the fluorescence of the supernatant was determined at 665 nm before and after acidification of the samples using a pre-calibrated TD-700 laboratory fluorometer (Turner Designs). On the basis of these measurements, Chl *a* concentration was calculated according to Arar and Collins (1997), taking into account the results from the blank filters.

SPE-DOS and DBC analyses

DOS was quantified in SPE-DOM extracts using methanolic extracts containing ~70 μg organic carbon. Aliquots were dried in an oven at 50°C and

redissolved in 2% HNO_3 (suprapur). Samples were measured with inductively coupled plasma optical emission spectrometry (ICP-OES) using a Thermo Scientific iCAP 6000 Series ICP. Dissolved black carbon (DBC) was quantified in SPE-DOM extracts, with high-performance liquid chromatography (UPLC) by detection of benzenepolycarboxylic acids (BPCA) as described previously (Dittmar 2008; Stubbins et al. 2012). For this study, only benzenepentacarboxylic acid (B5CA) and benzenhexacarboxylic acid (B6CA) were considered, because benzene rings substituted with three and four carboxylic acid groups (B3CA and B4CA) may be produced after the oxidation of non-pyrogenic organic matter (Kappenberg et al. 2016). Aliquots of the methanolic extracts containing 5 μmol organic carbon were dried at 50°C , redissolved with 500 μL of 65% HNO_3 (p.a.) and sealed in glass ampoules. For oxidation, the ampoules were heated to 170°C for 9 h. The HNO_3 was evaporated at 50°C using a centrifugal evaporator (RVC 2–18, Christ, Germany) equipped with a vacuum pump. The samples were redissolved with 100 μL phosphate buffer solution (5 mM NaH_2PO_4 and 5 mM Na_2HPO_4 , pH 7.2) and analyzed on a Waters Acquity UPLC (Ultra Performance Liquid Chromatography) system composed of binary solvent manager, a sample manager, a column manager, and a photodiode array light absorbance detector (PDA e λ).

Molecular DOM analysis

The molecular SPE-DOM composition was analyzed using FT-ICR-MS (solariX XR, Bruker Daltonik GmbH, Bremen, Germany), connected to a 15 Tesla superconducting magnet (Bruker Biospin, Wissembourg, France). Details on analytical conditions and molecular formulae assignment are provided in the supplementary material. All intensities of identified mass peaks with assigned molecular formulae within each sample were normalized to adjust different peak intensities to the same scale (0 to 1) between samples. The aromaticity index (AI_{mod}) and double-bond equivalents (DBE) were calculated after Koch and Dittmar (2016; 2006), and the intensity-weighted averages of the molar ratios (hydrogen-to-carbon, H/C; oxygen-to-carbon, O/C), DBE and AI_{mod} , as well as nitrogen (N), sulfur (S), and phosphorus (P) were calculated as previously described (Seidel et al. 2014). Compound groups were defined as described

in Merder et al. (2020): Aromatics ($AI_{\text{mod}} > 0.5$), highly unsaturated ($AI_{\text{mod}} < 0.5$, $H/C < 1.5$), unsaturated ($1.5 \leq H/C \leq 2$), unsaturated with N ($1.5 \leq H/C \leq 2$, $N > 0$) and saturated ($DBE = 0$). Only molecular formulae present in duplicate measurements were considered for further evaluation. The intensity-weighted relative abundances of the DOM compound groups (aromatic, highly unsaturated, unsaturated, unsaturated with N, saturated) were calculated. Furthermore, the normalized DOM molecular formulae data were used to calculate indexes to assess the degradation state of DOM (I_{DEG}) (Flerus et al. 2012), the presence of terrigenous DOM (I_{TERR}) (Lechtenfeld et al. 2014; Medeiros et al. 2016) and a novel molecular porewater DOM index (I_{SuP}) (Knoke et al. 2024). In brief, 40 molecular formulae identified by Medeiros et al., (2016) as marine molecular formulae (Mar) and 40 molecular formulae previously identified to be enriched in mangrove porewater samples (Map) were used to calculate the ratio of the sums of the normalized intensities (sum magnitudes Map/sum magnitudes (Map+Mar), which we refer to as I_{SuP}) (Knoke et al. 2024). The I_{TERR} by Medeiros et al. (2016) and I_{DEG} by Flerus et al. (2012) increase with higher contributions of terrestrial and degraded marine DOM, respectively. The I_{SuP} index increases with the increasing contribution of porewater-derived (terrestrial) DOM. The relative standard deviation of the DOM indexes and intensity-weighted averages of molar ratios in replicate measurements was $\leq 3\%$.

Dissolved trace metal analyses

Barium was measured by inductively coupled plasma-optical emission spectrometry (ICP-OES, iCAP 7400 Duo, Thermo Fisher Scientific) using matrix-matched external calibration and Sc as internal standard. The concentrations of dissolved Co, Mn, Mo, W, and Gd were measured by quadrupole inductively coupled plasma-mass spectrometry (Q-ICP-MS, iCAP Q, Thermo Fisher Scientific) coupled to a seaFAST pico pre-concentration and matrix removal module (Elemental Scientific) using kinetic energy discrimination (KED) mode with He as collision gas and external calibration as generally described in Dellwig et al. (2019, 2021). Masses of ^{157}Gd , and ^{184}W were corrected for polyatomic interferences by $^{141}\text{PrO}^+$, and $^{168}\text{ErO}^+$ by measuring a solution containing $20 \mu\text{g L}^{-1}$ of the interfering elements at the beginning of

each run. Corrections were smaller than 0.6%, and 0.1%, for ^{157}Gd , and ^{184}W because of low oxide formation rates in KED mode. Precision and trueness of ICP measurements were determined with the reference materials NASS-7, CASS-6, SLEW-3 and SLRS-6 (NRCC) and were better than 9% and -10%, respectively (except for W in CASS-6 with a trueness of +15%). Because no certified values are available for Ba, W and rare earth elements (REE) we used published data (Ebeling et al. 2022) and a mean of own measurements for Ba (details in Supplementary Table S2).

Statistical analysis

The DOM molecular formulae from normalized FT-ICR-MS data were used to perform a principal coordinate analysis (PCoA) on a Bray Curtis dissimilarity matrix using the R statistical platform (R core team 2022) as described in Seidel et al. (2017). The parameters of the DOM molecular data, environmental data, dissolved trace metals, as well as FDOM, DBC and SPE-DOS measurements were centered (mean=0, standard deviation=1) and then fitted post-hoc to the PCoA scores using the *envfit* function of the *vegan* package (Oksanen et al. 2022) within the R statistical platform (R core team 2022) as described by Seidel et al. (2017). The correlation of the parameters to the DOM molecular composition (PCoA) was tested with 10,000 permutations and was considered significant if $p < 0.1$. The vectors represent correlations of the parameters with the sampling points and close spatial arrangement in PCoA plots visualizes sample similarity. Perpendicular projections of sampling points onto vector arrows depict maximum correlations with the molecular parameters. In the PCoA, the sample stations were grouped with colors in DOM clusters, based on a Bray Curtis dissimilarity matrix (*vegdist*) using Ward's hierarchical clustering (*hclust*). Surface plots and maps were produced using Ocean Data View (Schlitzer 2022).

Conservative mixing analyses

To evaluate the different contributions of the three main rivers draining into the German Bight, we performed conservative two-endmember mixing analyses for the concentrations of dissolved trace metals, DOC, SPE-DOS, DBC, NO_3^- , NO_2^- , DIP and DSi,

and the relative fluorescence of humic-like FDOM. The mixing analysis was performed separately with three estuarine endmembers because the riverine endmembers at near-zero salinity were not covered (stations: Elbe 03 with salinity 1.3, Ems 04 with salinity 12.9, Weser WS01 with salinity 5.2) and the two offshore endmember stations ES01 and ES02 (samples 591 and 593 in Supplementary Table S1). To evaluate how the relative values of the I_{TERR} and I_{SuP} indexes, DOS/DOC ratio and average sulfur content of molecular formulae (from FT-ICR-MS) deviated from values expected from conservative mixing along the estuarine to North Sea gradient, we further calculated the theoretical values assuming fully conservative mixing. As a first step, we calculated the (linear) two-endmember conservative mixing scenarios for the numerators and denominators of the various ratios. As a second step, we divided the respective computed values for a given endmember mixing ratio, as determined via salinity. Ratios and molecular DOM indices do not mix linearly and follow a curved trend when plotted against salinity.

Results

Bulk geochemical parameters

As expected, the lowest salinity was observed in the estuaries (Fig. 2a; Supplementary Table S1). Further offshore, salinity increased to open ocean levels around 35. The pH was also lowest in the estuaries of the rivers Elbe and Ems and increased offshore (Fig. 2b; no pH for Weser estuary available). Saturation of DO was lowest in the Ems estuary at 73% and increased in the North Frisian region and offshore to 94% (Fig. 2c). The concentrations of DO were highest in the Elbe estuary and lowest in the Ems estuary (Fig. 2d).

Concentrations of Chl *a* were highest in Elbe and Ems River mouths (no data for Weser River mouth; Fig. 2e). Lower values were found in the North Frisian region and offshore (Fig. 2e). Relative humic-like FDOM fluorescence was highest in the estuaries and decreased offshore (Fig. 2f; Supplementary Table S3). Likewise, concentrations of DOC were highest in the estuaries and close to the North Frisian region and decreased offshore (Fig. 2g).

Concentrations of TDN were highest in the estuaries and close to the North Frisian region and decreased offshore (Fig. 2h; Supplementary Table S3). Concentrations of NO_2^- and NO_3^- were highest in the less saline reaches of the rivers Elbe, Ems and Weser and strongly decreased offshore, with values often falling below the limit of detection (LOD NO_2^- 0.16 μM and NO_x 1 μM ; Supplementary Fig. S1a, b). Highest DIP and DSi concentrations again appeared in the Elbe, Weser and Ems estuaries, whereas lowest levels were observed during tidal cycles and offshore transects (LOD DIP 0.1 μM and DSi 0.3 μM ; Supplementary Fig. S1c, d). High SPE-DOS concentrations were measured in the estuaries with a maximum in the Ems estuary (Supplementary Fig. S1e), and lower values in the North and East Frisian areas, and the offshore stations. The S/C ratio (DOS/DOC ratio in SPE-DOM, in %) ranged from 0.6 to ~1% in the estuaries, the North and East Frisian area and were lowest offshore (Supplementary Fig. S1f). Concentrations of DBC were lowest offshore and highest in the estuaries (Fig. 3a). The B6CA/B5CA values, percentage of DBC in DOC (Fig. 3b, c), as well as concentrations of B5CA and B6CA (Supplementary Fig. S1g, h) were higher close to the coast and in the rivers compared to offshore stations.

Mixing analysis revealed nearly conservative behavior for DOC, FDOM, SPE-DOS, DBC, NO_3^- and DSi (Fig. 4), whereas NO_2^- and DIP were above the values expected from conservative mixing (Fig. 4). Tidal cycle sampling at station S2 close to the tidal inlet Otzumer Balje (Fig. 1c) covered diurnal cycles (indicated, for example, in Supplementary Figs. S2, S3, S4). A noticeable relationship of the measured parameters with day-night-cycles was not observed, except for Chl *a* and the concentration and saturation of DO (Supplementary Fig. S2e–g). Salinity varied between 29.8 (low tide) and 30.9 (high tide) during the tidal cycle sampling (Supplementary Fig. S2). Concentrations of DOC, TDN, relative fluorescence of FDOM (Supplementary Fig. S2a–c), NO_2^- , NO_3^- , SPE-DOS (Supplementary Fig. S3a–c), DBC, B5CA, B6CA, and relative abundance of DBC (%DOC) (Supplementary Fig. S4a–e) were highest at low tide, whereas pH values (Supplementary Fig. S2d) were lowest at low tide. Values of S/C of SPE-DOM (Supplementary Fig. S3d), B6CA/B5CA (Supplementary Fig. S4b), Chl *a* (Supplementary Fig. S2e), and DO saturation and concentration

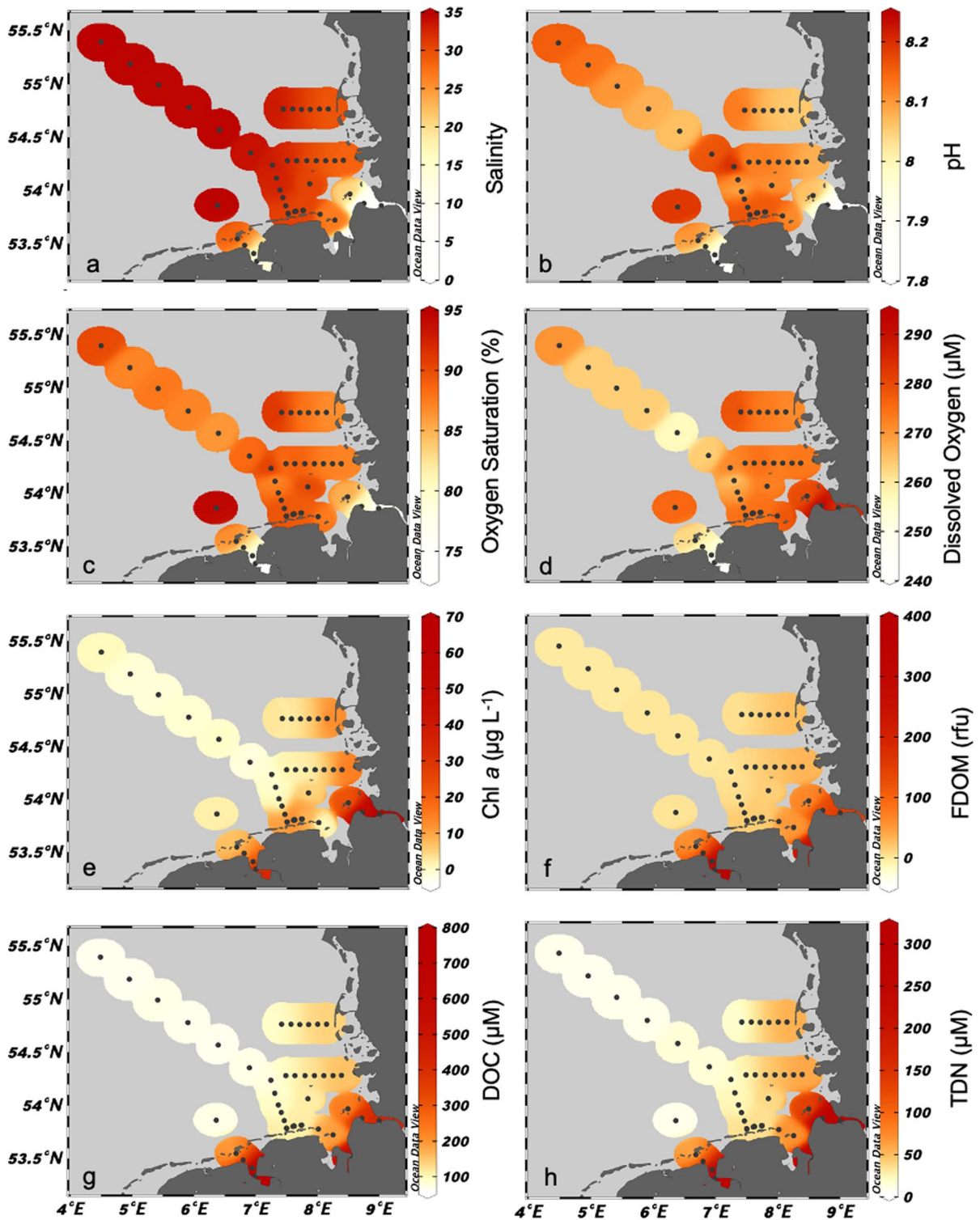


Fig. 2 Distribution of salinity (a), pH values (b), oxygen saturation (c), concentrations of dissolved oxygen (d), concentrations of chlorophyll *a* (e), FDOM in relative fluorescence units

(rfu) (f), dissolved organic carbon (DOC) (g), and total dissolved nitrogen (TDN) (h). Black circles represent sampling stations in the German Bight

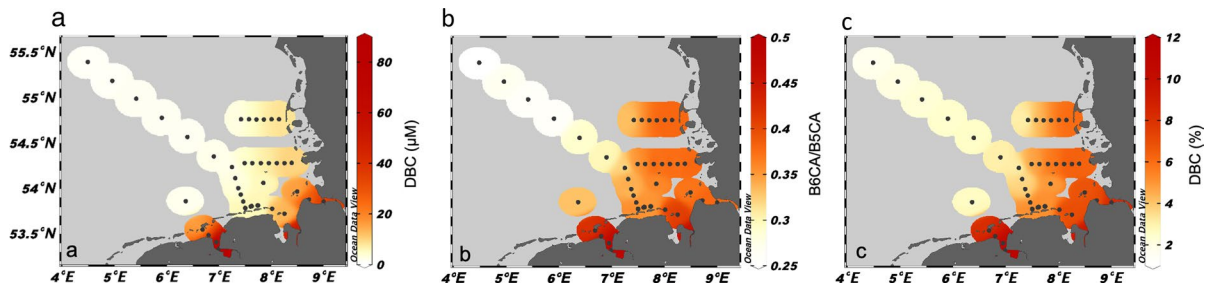


Fig. 3 Distribution of concentrations dissolved black carbon (DBC) (a), the ratio of benzenepentacarboxylic acid (B5CA) and benzenhexacarboxylic acid (B6CA) (B6CA/B5CA) of

DBC (b), and the percentage of dissolved black carbon (DBC) in dissolved organic carbon (DOC) (c) in the German Bight. Black circles represent sampling stations

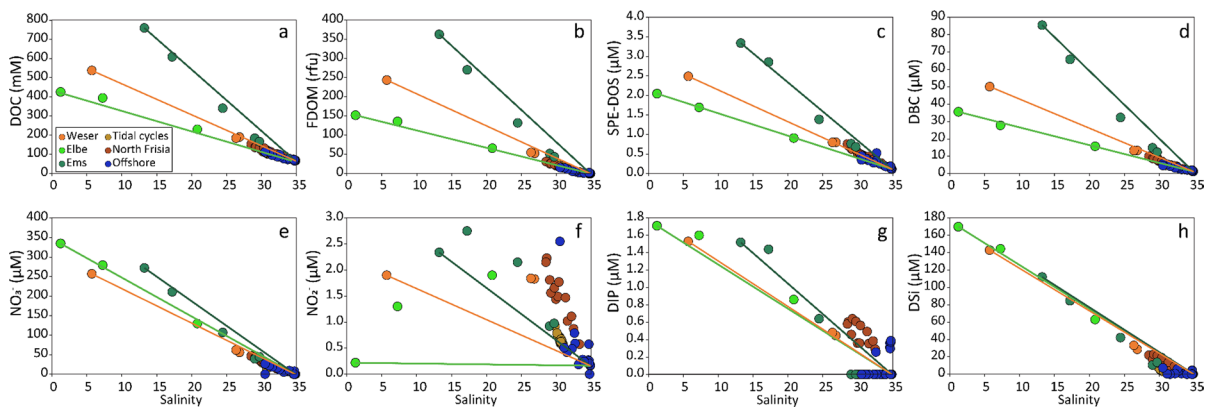


Fig. 4 Mixing plots of bulk and DOM surface water parameters versus salinity. Solid lines indicate the theoretical conservative mixing line between estuarine and marine endmembers of bulk parameters: dissolved organic carbon (DOC) (a), fluorescent dissolved organic matter (FDOM) (b), solid-phase

extractable dissolved organic sulfur concentrations (SPE-DOS) (c), dissolved black carbon (DBC) (d), nitrate (NO_3^-) (e), nitrite (NO_2^-) (f), dissolved phosphate (DIP) (g), and dissolved silicate (DSi) (h). “Offshore” data points include the Offshore and Transition cluster stations

(Supplementary Fig. S2f, g) showed no clear tidal patterns.

Dissolved trace metals

Concentrations of the dissolved trace metals Ba, Co, Mn, Gd, and W were elevated in the estuaries compared to the adjacent East and North Frisian coastal areas and showed lowest levels offshore (Fig. 5, Supplementary Fig. S5; Supplementary Table S4). The concentrations of dissolved Gd and W were highest in the low salinity reaches of the Elbe estuary, whereas Ba, Co, and Mn were highest in the Weser estuary. In contrast, Mo revealed an expected opposite behavior with an ocean-like level between 91 and 103 nM in the offshore region decreasing to a

minimum concentration of 11.7 nM in the Elbe estuary at a salinity of 1.2 (Supplementary Fig. S5f). Dissolved Mn showed negative deviations from conservative behavior, whereas dissolved Ba, Co, as well as W, and Gd revealed positive deviations regarding the estuarine Weser and Elbe endmembers, respectively (Fig. 5). Dissolved Ba, Co and Gd revealed a tidal pattern with highest concentrations during low tide (Fig. 6), which was less pronounced for Mn. In contrast, dissolved W and Mo showed no clear tidal patterns (Fig. 6e, f). There was no noticeable relationship of the measured parameters with day-night-cycles. Positive anomalies of Gd (compared to Post Archean Australian Shale, PAAS, rock reference material) (e.g., Nance and Taylor 1976) due to anthropogenic contribution were found in all three

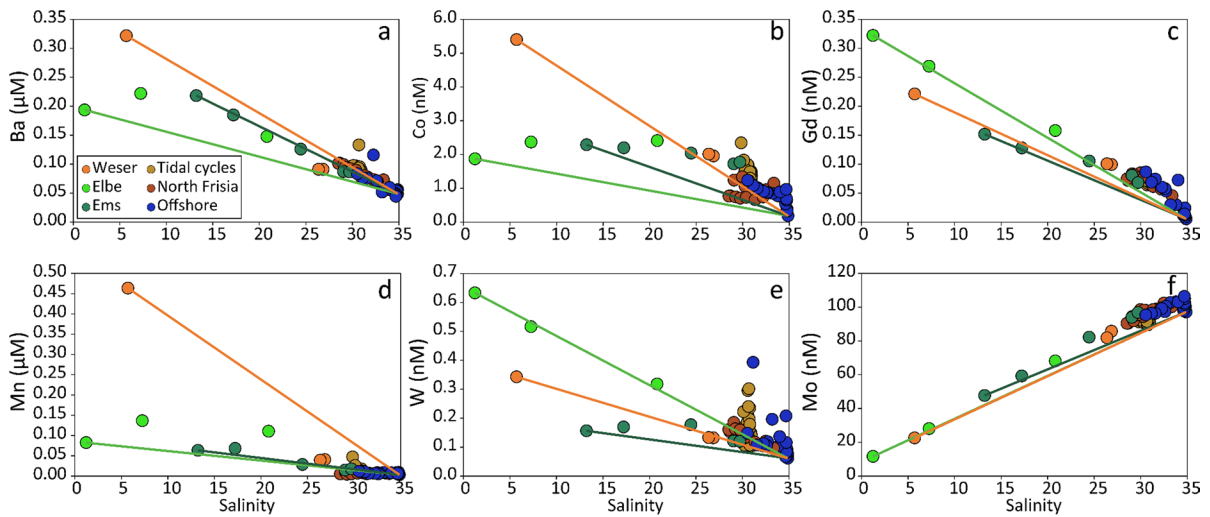


Fig. 5 Mixing plots of dissolved trace metals versus salinity. Solid lines indicate the theoretical conservative mixing line between estuarine and marine endmembers of dissolved trace metals: barium (Ba) (a), cobalt (Co) (b), gadolinium (Gd) (c),

manganese (Mn) (d), tungsten (W) (e), and molybdenum (Mo) (f) in the German Bight. “Offshore” data points include the Offshore and Transition cluster stations

estuaries and were most pronounced for the on average less saline samples of the Elbe estuary (Supplementary Fig. S6).

DOM molecular characterization

The total number of assigned molecular formulae was 12,748, ranging between 3270 and 8445 per sample (Supplementary Table S5). Intensity-weighted averages of aromaticity (AI_{mod}) molecular formulae were highest in the estuaries and decreased offshore (Supplementary Fig. S7a, Table S5). Accordingly, intensity-weighted averages of H/C values were highest offshore and lowest in the estuaries (Supplementary Fig. S7b). In contrast to the Elbe and Weser estuaries, intensity-weighted averages of the O/C values were highest in the Ems estuary, offshore and North Frisia (Supplementary Fig. S8b). The intensity-weighted averages of molecular masses (m/z) were between 380 and 447 Da. Lower masses were found in tidal cycle and estuarine samples, whereas higher masses appeared offshore (Supplementary Table S5). Intensity-weighted averages of the N-content in molecular formulae were lowest in the estuaries and highest offshore (Supplementary Fig. S7d). In contrast, the S-content was highest in the estuaries and near the

North Frisian sampling stations, with decreasing values offshore (Supplementary Fig. S7c).

Values of I_{Terr} and I_{Sup} were highest in the estuaries and decreased offshore (Supplementary Fig. S7e, f). In contrast, I_{Deg} values were highest offshore and lowest at the North and East Frisian Wadden Sea stations (Supplementary Table S5). Highest intensity-weighted abundances of aromatic compounds were found in the estuaries (Supplementary Fig. S8a; Supplementary Table S6). The intensity-weighted relative abundances of highly unsaturated compounds increased from the Elbe estuary to the offshore realm (Supplementary Fig. S8c). Unsaturated compounds and unsaturated compounds containing N increased from the estuaries to the North Frisian and offshore stations (Supplementary Fig. S8d, e).

The I_{Terr} index showed mostly conservative mixing behavior for the combined Elbe and Weser but pronounced positive deviations for the Ems stations (Fig. 7a). The I_{Sup} index showed mostly conservative behavior including the river Ems (Fig. 7b). The DOS/DOC values of SPE-DOM and the average S-content of molecular formulae (from FT-ICR-MS) showed a non-conservative behavior with strong positive deviations especially at a salinity > 25, i.e., in samples from the tidal cycle (East Frisia), North Frisia and offshore (Fig. 7c, d).

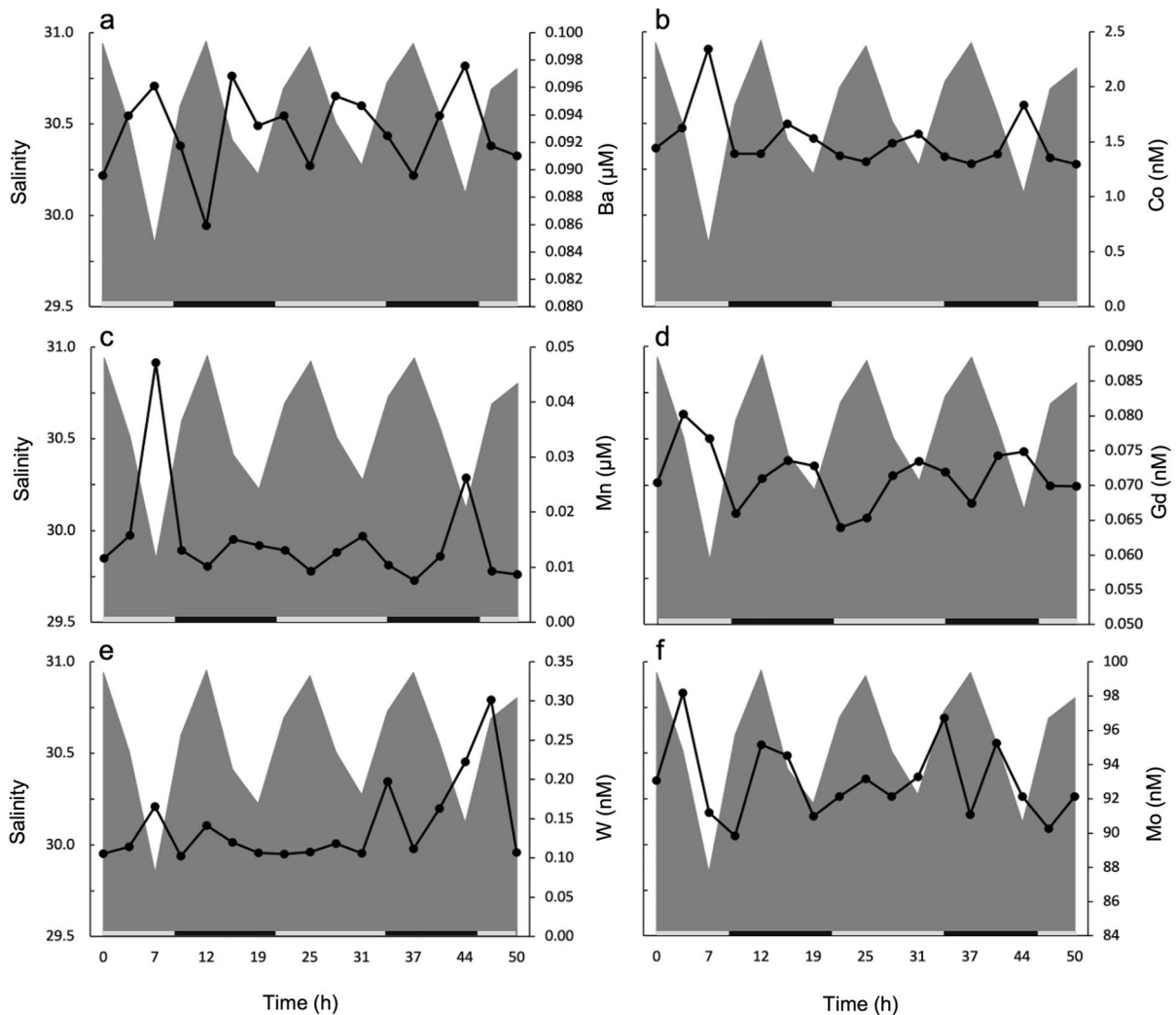


Fig. 6 Tidal cycle sampling at station S02 in the Oetzumer Balje (Fig. 1c) over ~50 h. The gray area represents salinity. The black data points connected by lines show the concentrations of dissolved barium (Ba) (a), cobalt (Co) (b), manganese

(Mn) (c), gadolinium (Gd) (d), tungsten (W) (e), and molybdenum (Mo) (f) in the German Bight. Day-night cycles are indicated by white-black bars on the time axis

We did not observe a clear trend for the saturated DOM group (Supplementary Fig. S8f). Values of I_{Terr} , I_{SuP} , AI_{mod} , intensity-weighted averages of H/C, and N- and S-content were generally highest during low tide and lowest during high tide (Supplementary Fig. S9). In contrast, values of I_{DEG} and O/C were highest at high tide and lowest at low tide (Supplementary Fig. S9c, e).

Statistical analysis

We analyzed the relationship between DOM molecular composition, environmental parameters, and trace metal concentrations using PCoA (Figs. 8, 9, 10) in combination with cluster analysis (Supplementary Figs. S10, S11). The first two PC axes, explaining 68% variability, revealed distinct clusters: River 1

Fig. 7 Conservative mixing plots of the terrestrial index (I_{TERR}) (a), porewater-derived DOM index (I_{SUP}) (b), dissolved organic sulfur to dissolved organic carbon (DOS/DOC) (c) and average sulfur content in molecular formulae (d). Solid curves indicate the theoretical conservative mixing between estuarine and marine endmembers in the German Bight. Note that for ratios and relative abundances conservative mixing results in a non-linear relationship with salinity. “Offshore/Transition” data points include the Offshore and Transition cluster stations

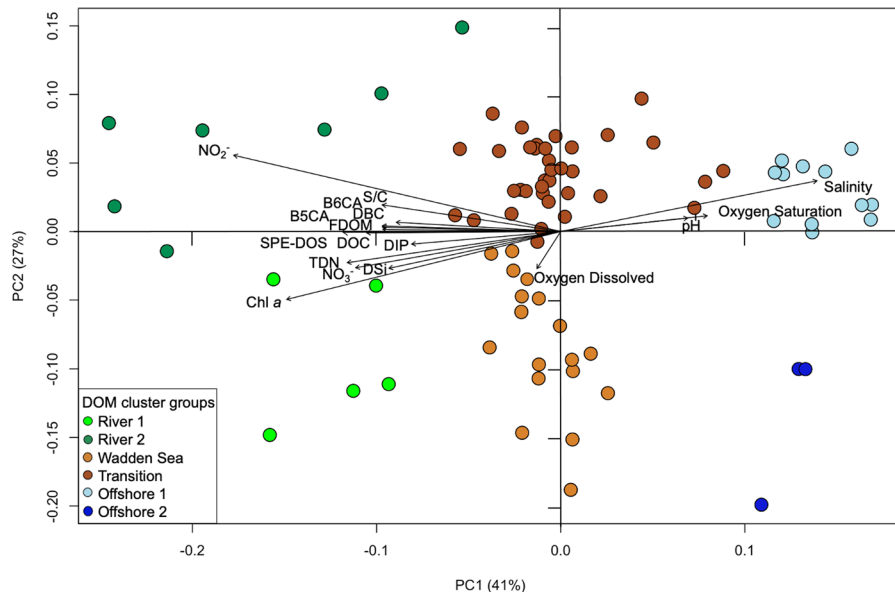
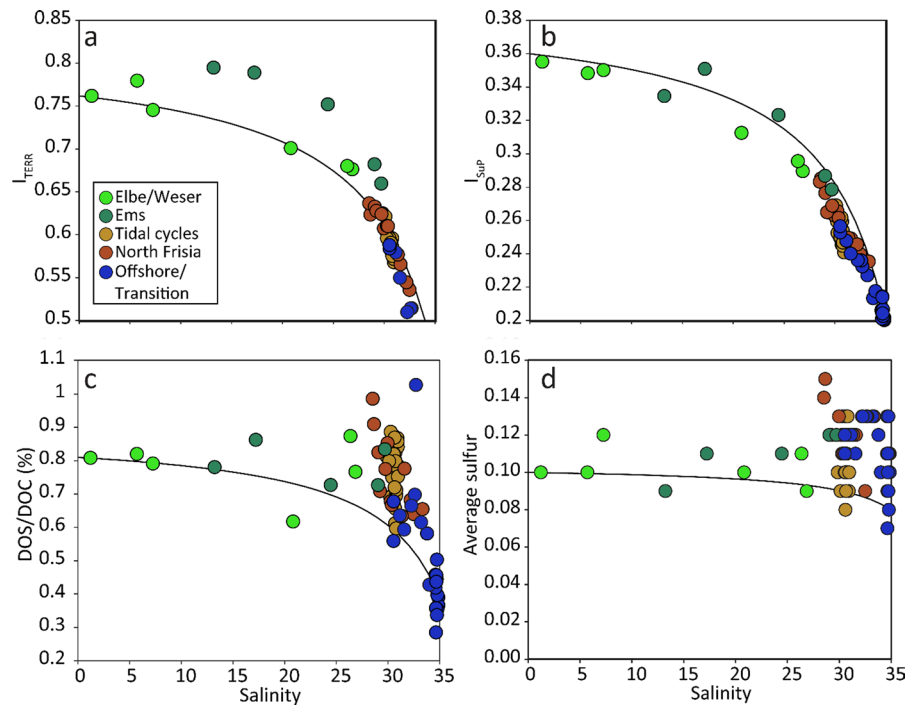


Fig. 8 PCoA based on Bray–Curtis dissimilarities of the relative abundance of DOM molecular formulae. The percentages give the DOM molecular variability as explained by the axes (PC1 and PC2). The colored dots represent the sample stations that can be grouped into six different DOM clusters: River 1,

River 2, Wadden Sea, Transition, Offshore 1, and Offshore 2. The environmental parameters were fitted onto the ordination posthoc (black arrows) and were considered significant with $p \leq 0.1$. Station numbers and cluster analysis are shown in Supplementary Figures S10 and S11

Fig. 9 PCoA based on Bray–Curtis dissimilarities of the relative abundance of DOM molecular formulae with sample stations clustered as in Fig. 8. DOM compound groups (aromatic, saturated, unsaturated, highly unsaturated, and unsaturated with nitrogen), values of aromaticity (AI_{mod}), number of molecular formulae (number), intensity-weighted averages of molecular masses (m/z), sulfur (S), nitrogen (N), O/C and H/C ratios, as well as I_{Terr} , I_{SuP} , and I_{DEG} indexes were fitted onto the ordination posthoc (black vectors, considered significant with $p \leq 0.1$)

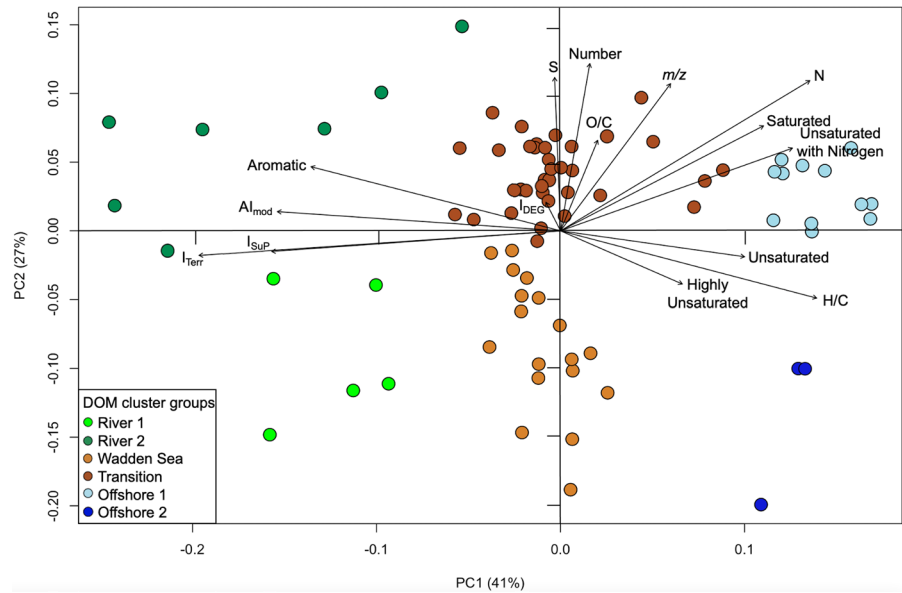
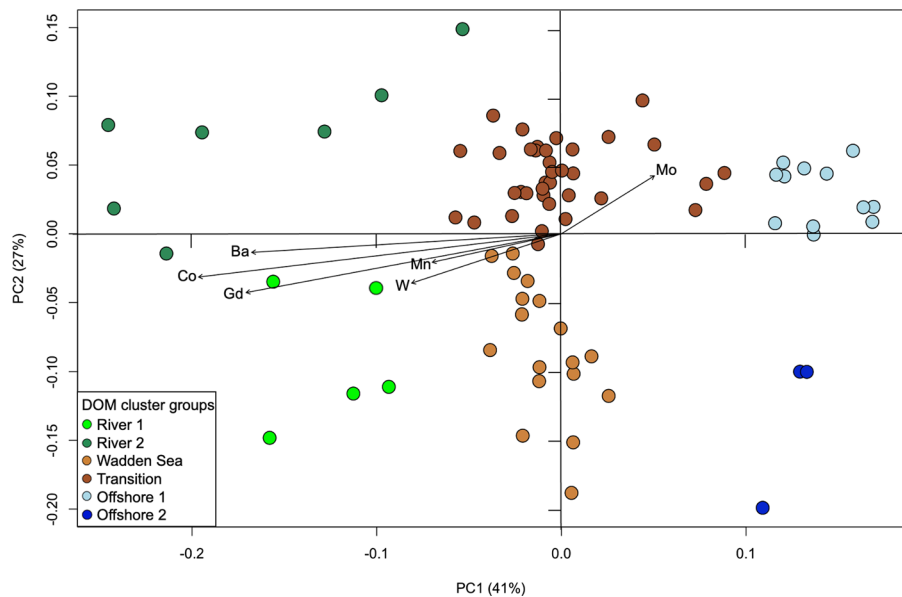


Fig. 10 PCoA based on Bray–Curtis dissimilarities of the relative abundance of DOM molecular formulae with sample stations clustered as in Fig. 8. Dissolved trace metals molybdenum (Mo), barium (Ba), cobalt (Co), manganese (Mn), tungsten (W), and gadolinium (Gd) were fitted posthoc onto the ordination (black vectors, considered significant with $p \leq 0.1$)



(Elbe and Weser estuaries), River 2 (Ems estuary), North and East Frisian Wadden Sea, Transition, Offshore 1, and Offshore 2 (Fig. 8). The explained variability was 6% for PC3 and 3% for PC4. We did not identify significant trends with environmental parameters other than those that were explained by PC1 and PC2. PC1 separated the Offshore from the River clusters, while PC2 separated River and Offshore clusters, as well as the Wadden Sea cluster from

the Transition cluster. PC1 was correlated to salinity, DOC, DBC, SPE-DOS, FDOM, and S/C values. The parameters salinity, DO saturation, and pH were related to the Offshore clusters, whereas Chl *a*, DSi, NO_3^- , TDN, and DIP concentrations were associated with the River 1 cluster, and NO_2^- with the River 2 cluster (Fig. 8). River clusters were further related to aromatic compounds, AI_{mod} , I_{Terr} , and I_{SuP} values (Fig. 9). The Transition cluster was related to higher

molecular formulae counts, S-content, O/C, and I_{DEG} values. Finally, the Offshore 1 cluster was related to saturated and N-containing compounds, whereas Offshore 2 cluster was related to unsaturated and highly unsaturated DOM compounds, as well as H/C values (Fig. 9). The dissolved trace metals Ba, Co, Gd, Mn, and W were linked to the River clusters, while Mo concentrations were associated with Offshore clusters (Fig. 10).

Discussion

Biogeochemical dynamics of nutrients and bulk parameters in the German Bight

In the German Bight, rivers significantly influence physicochemical parameters and the distribution patterns of nutrients, including dissolved nitrogen species, phosphate, and silicate. Additional dynamics are associated with both porewater inputs and biological activity. The patterns of salinity and pH in the southern German Bight reflect the mixing of river-derived freshwater and the inflow of North Atlantic seawater (Fig. 2a, b) (Carstensen and Duarte 2019;

Francescangeli et al. 2021; Painter et al. 2018). High algal biomass as reflected by Chl *a* (Fig. 2e) coincided with higher nutrient concentrations such as TDN (Fig. 2h), DIP, and DSi (Supplementary Fig. S1) close to the coast and estuaries, thereby demonstrating the importance of riverine input and porewater outwelling for coastal primary production. The rivers of the southern North Sea carry high N loads due to anthropogenic and agricultural activities (Brockmann et al. 2018; Howarth 1998) (see conceptual Fig. 11). In our sample set, areas with elevated DOC concentrations typically displayed higher levels of TDN and NO_2^- as well as lowest degrees of DO saturation due to intensified heterotrophic respiration stimulated by organic matter and nutrient input (Abril and Frankignoulle 2001; Dai et al. 2006; Nezlin et al. 2009).

Comparable concentrations of NO_3^- and TDN (Supplementary Fig. S1b, Fig. 2h), identified NO_3^- as the dominating TDN compound. Ammonium concentrations are generally low in the oxic North Sea water column since it is rapidly oxidized and quickly consumed by phytoplankton (Domingues et al. 2011; Laperriere et al. 2019). Porewater outwelling primarily provides NH_4^+ , which is then oxidized to

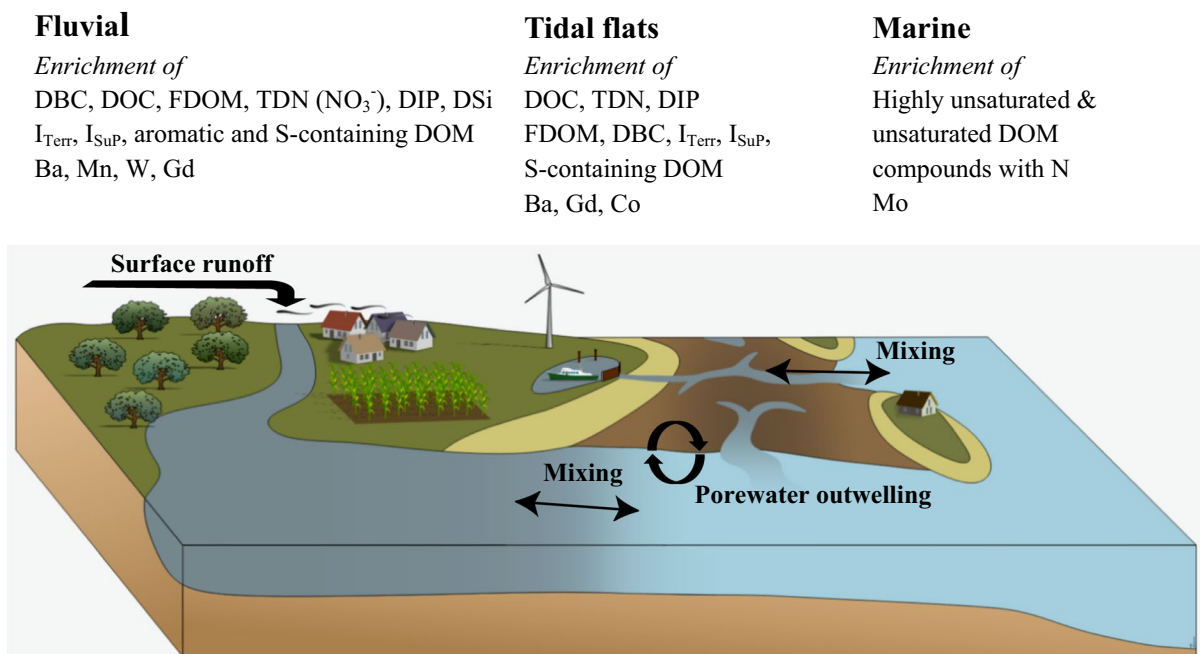


Fig. 11 Conceptual representation of the enrichment of geochemical parameters in the sampling area of the German Bight

NO_2^- in the water column. Highest concentrations of NO_2^- along the North Frisian transects and in the estuaries (Supplementary Fig. S1a) were thus likely due to outwelling of O_2 -depleted porewater from sediments (Beck and Brumsack 2012; Sanders and Laanbroek 2018). Porewater sources were further confirmed by both, tidal cycle sampling with highest concentrations of NO_2^- during low tide when porewater outwelling is highest (Beck et al. 2020; Grunwald et al. 2010; Seidel et al. 2014) (Supplementary Fig. S3) and the mixing analysis with positive deviations from non-conservative behavior at high salinity for NO_2^- and DIP (Fig. 4f, g). Phosphate is released during reduction of sedimentary iron(hydro)oxides, supplementing the contribution of DIP via remineralization of algal material (Beck et al. 2020).

Similarly, elevated DSI concentrations close to the coast originate from both riverine input (Beusen et al. 2009) and the contribution by generally DSI-rich porewaters with the latter again confirmed by high levels during low tide (Supplementary Fig. S3e) (Beck et al. 2008a; Grunwald et al. 2010; Seidel et al. 2014; Oehler et al. 2019). In winter with low phytoplankton biomass, DSI concentrations are around 20 to 30 μM in the water column of the tidal inlet of Spiekeroog Island (Otzumer Balje, Fig. 1c) (Beck et al. 2020), whereas we found concentrations even below 5 μM (Supplementary Fig. S3e). Thus, our sampling was conducted at the onset of the spring phytoplankton bloom, and negative deviations of DSI concentrations from conservative mixing therefore suggest removal by diatoms (Beck et al. 2020; Grunwald et al. 2010; Kowalski et al. 2012).

Tidal flats as important source of trace metals in the German Bight

In the German Bight, redox-sensitive trace metals, except for Mo, exhibited highest concentrations near the coast due to the input via estuaries and porewater outwelling.

The spatial distribution of Mo in the German Bight can be explained by the dilution of Mo-rich seawater with comparatively Mo-poor river water (Fig. 5f). Additionally, Mo concentrations are depleted in the coastal North Sea due to sequestration in sulfidic sediments and by adsorption onto organic particles (Beck et al. 2008a; Cole et al. 1993; Riedel et al. 2011; Smedley and Kinniburgh 2017). Substantial

Mo-depletion in the water column, as frequently observed after summer algae blooms due to formation of large aggregates that become enriched in Mo (Dellwig et al. 2007a; Kowalski et al. 2013), can be excluded due to the timing of our sampling campaign in early spring. Thus, sequestration in sulfidic tidal flat sediments is the dominant process controlling Mo concentrations in nearshore waters during our sampling campaign. This is reflected by depleted Mo concentrations in the water column during low tide when Mo-depleted porewater is discharged (Fig. 6f).

Dissolved Ba concentrations are generally higher in coastal waters than in the surface ocean due to the desorption of Ba from sediments and riverine suspended matter (Moore 1997; Coffey et al. 1997; Moore et al. 2011; Samanta and Dalai 2016). Furthermore, it originates from tidal flat sediments in the Wadden Sea (Riedel et al. 2011; Seidel et al. 2014) as demonstrated by increased concentrations during low tide when porewater outwelling is highest (Fig. 6a). Similarly, porewater outwelling delivers Mn and Co to coastal waters of the North Sea (Fig. 6b, c) since in oxygen-depleted intertidal sediments Mn (hydr-) oxides are reduced leading to the release of dissolved Mn and formerly scavenged Co, with the latter also being released during the degradation of Co-containing organic complexes (Sundby et al. 1986; Tribovillard et al. 2006). The spatial concentration pattern of Co (Supplementary Fig. S5b) is further controlled by its low open ocean concentration and its short oceanic residence time due to its removal from solution by interaction with (estuarine) particles (Byrd et al. 1990; Saito et al. 2002; Saito and Moffett 2002) and marine phytoplankton (Saito et al. 2002; Sunda and Huntsman 1995).

Highest W concentrations close to the North Sea coast and in the Elbe estuary (Supplementary Fig. S5e) indicate anthropogenic sources (Francescangeli et al. 2021). Lower W concentrations offshore are due to the dilution with W-depleted seawater (Mohajerin et al. 2016) and removal due to interactions with sinking particles and Fe/Mn (hydr-) oxides (Kashiwabara et al. 2013). Studies conducted in hypoxic-euxinic basins of the Baltic Sea, Black Sea, and the Mississippi River delta reported strong W enrichments in sulfidic porewater due to the elevated solubility of thiolated W (Dellwig et al. 2019; Mohajerin et al. 2016) suggesting porewater outwelling as an important source to the open water

column. However, the weakly pronounced tidal W dynamics in our study do not clearly support this assumption, which might be due to sulfide levels in the porewater that were insufficiently high allowing elevated thiolation and thus an increased W solubility during our sampling period (Fig. 6e). In addition, the strong affinity of W to Mn oxide minerals (Kashiwabara et al. 2017) that are present in the uppermost sediment layer of the tidal flats especially during winter and early spring (Dellwig et al. 2007b), may also trap some of the porewater W tending to escape the from the sediments.

The densely populated Elbe estuary had the most pronounced Gd anomaly (Supplementary Fig. S6) compared to the Weser and Ems, and thus the highest anthropogenic impact if salinity-related variations are excluded (Kulaksiz and Bau 2007). Although complexed Gd is mainly derived from the anthropogenic sources, it was suggested that Gd can also enter the water column in its non-complexed form via porewater reflux following release of scavenged Gd after degradation of organic complexes and/or Fe/Mn-(hydr-)oxides (Paffrath et al. 2020) (Fig. 6d).

Combined analysis deciphers tidal flats as important DOM sources in the German Bight

Rivers generally contribute large proportions of (chromophoric) DOM to the southern North Sea (Lübben et al. 2009; Painter et al. 2018) leading to higher DOC concentrations and terrestrial, humic-like FDOM values in the estuaries (Fig. 2f). Humic-like FDOM in backbarrier tidal flats can be attributed to degraded terrestrial material such as peat in the sediment (Seidel et al. 2014). Additionally, porewater outwelling, as demonstrated in the tidal cycle sampling (Supplementary Fig. S2a, c), and freshwater discharge from small fluvial watercourses draining the hinterland transport terrestrial DOM to the coastal North Sea (Lübben et al. 2009; Seidel et al. 2015a; Waska et al. 2019).

We observed only small negative deviations of DOC concentrations and humic-like FDOM values from conservative mixing (Fig. 4a, b) suggesting minor removal of terrestrial DOM through bio-degradation, flocculation, and photo-bleaching in the offshore areas (Medeiros et al. 2015b; Osterholz et al. 2016; Stubbins et al. 2010). In general, terrestrial DOM is characterized by high aromaticity (AI_{mod})

and low H/C values (Abdulla et al. 2013; Osterholz et al. 2016; Seidel et al. 2015b; Sleighter and Hatcher 2008). In our study, the Ems estuary exhibited the highest abundances of aromatic DOM, aromaticity (AI_{mod}), and DBC concentrations compared to the rivers Weser and Elbe (compare cluster River 1 to River 2, Fig. 8, and Fig. 9). This indicated a greater relative contribution of (highly) aromatic DOM from the Ems River to the coastal North Sea compared to the other two rivers. This can be attributed to extensive peat bogs in its watershed (Houben et al. 2021) and the high turbidity of the Ems River, which protects terrestrial aromatic DOM from photo-degradation in the water column. Overall, the German Bight region had spatially evenly distributed AI_{mod} values, indicating the export of relatively stable riverine DOM to the open North Sea. The distribution pattern of I_{Terr} values (from FT-ICR-MS), an indicator for terrestrial DOM, supported this observation (Supplementary Fig. S7e).

The relationship of H/C values and abundance of unsaturated aliphatic compounds containing N with the Offshore cluster on the one hand and Wadden Sea stations on the other hand (Fig. 9) indicated a shift from terrestrial to more marine (algal) DOM, which has higher H/C levels and contains more N compared to terrestrial DOM (Medeiros et al. 2015b; Sleighter and Hatcher 2008). Furthermore, the O/C and I_{DEG} values, indicators of degraded DOM (Flerus et al. 2012), were inversely related to the Wadden Sea cluster, suggesting that the DOM contributed via outwelling of anoxic porewater from the intertidal flats contains less oxygenated and potentially less degraded marine DOM compared to the coastal North Sea (Transition stations, Fig. 9). The lack of oxygen in sediments probably inhibits heterotrophic degradation of DOM (Burdige et al. 2016) explaining the accumulation of less oxygenated, and recalcitrant DOM (including DOS and DBC) in anoxic intertidal flats.

Highest concentrations of DBC were found in the estuaries, especially the Ems (Fig. 3a), identifying rivers as the main pathway for DBC transport from land to sea (Jaffé et al. 2013). The nearshore North Frisian area also exhibited high DBC concentrations, likely associated with the Elbe River plume that is transported northward by the clockwise circulation in the southern North Sea (Fig. 3a). However, the tidal cycles revealed that DBC concentrations were highest

at low tide (Supplementary Fig. S4a), suggesting tidal flats as an additional source (Seidel et al. 2014). On the other hand, in the high salinity range, no positive deviations from conservative mixing of DBC concentrations were observed, implying a balance between the removal of riverine DBC and the input of porewater-derived DBC (Fig. 4d). Since DBC is resistant to biological degradation, its concentrations at offshore stations with increased light penetration were likely reduced through photo-degradation (Stubbins et al. 2012), and dilution with low DBC-seawater. The B6CA/B5CA values, which decreased from coastal regions and estuaries towards offshore, suggested a change in DBC condensation (Fig. 3b). This decrease is probably due to preferential photodegradation of the more condensed and photosensitive B6CA, resulting in less aromatic DBC (Stubbins et al. 2012).

Dissolved Ba, Co, Gd, Mn, and W concentrations were associated with the River 1 cluster (Weser and Elbe Estuaries, Fig. 10), with particularly high Gd concentrations in the Elbe estuary (Supplementary Fig. S5d). Although Gd was intended as a tracer for anthropogenic riverine input, the release of previously scavenged Gd from tidal flats should be considered as well. Nonetheless, tidal cycles and positive deviations from conservative mixing of dissolved Gd, but also Ba, Co, and W, were in line with the relative enrichment of DOS at salinity > 25 indicating tidal flats as important sources.

Higher SPE-DOS concentrations in the estuaries confirmed rivers as the main sources for the southern North Sea. The Ems estuary exhibited highest SPE-DOS concentrations, likely due to its hyper-turbid state with limited photo-degradation and resuspension of sulfidic estuarine sediments (Winterwerp et al. 2017). Although bacterial sulfate reduction and thus sulfide production might be hampered in rivers due to lower sulfate concentrations compared to seawater (Ehlert von Ahn et al. 2023), additional input of SPE-DOS occurs from agricultural and urban sources (Osterholz et al. 2016; Wagner et al. 2015), and potentially from sulfidic peats observed in the Ems River watershed (Houben et al. 2021). Furthermore, the close relationship between the I_{Terr} and I_{SUP} indexes (Fig. 9), which represent terrestrial and sulfidic porewater DOM, respectively, indicated that porewater DOM in sulfidic estuarine sediments shares similar molecular properties with sulfidic intertidal sediments. Likewise, correlations of SPE-DOS and

dissolved Mn concentrations (Figs. 8, 10) suggested similar sources, i.e., estuaries and porewater, respectively. Concentrations of SPE-DOS mixed mostly conservatively in the German Bight (Fig. 4c), but microbial (Ksionzek et al. 2016; Longnecker et al. 2020) and photo-degradation (Gomez-Saez et al. 2017) are potential sinks further offshore.

The elevated SPE-DOS concentrations along the North Frisian coast compared to the offshore stations (Supplementary Fig. S1e), were possibly derived from the Elbe River plume that moves along the eastern North Sea coast (Callies et al. 2017). However, high S/C values of SPE-DOM near the North Frisian coast (S/C ~ 1, Supplementary Fig. S1f) suggested additional sulfur-enriched DOM input from nearby intertidal flats. This assumption is supported by higher concentrations of SPE-DOS and S-containing DOM molecular formulae during low tide (Supplementary Fig. S3c, Fig. S9h). Similar to the North Frisian coast, our tidal sampling station at the East Frisian coast also receives diluted (Ems) river water due to clockwise circulation in the North Sea (Rehder et al. 1998). However, conservative mixing analysis revealed sulfur-enriched DOM from sulfidic intertidal flats as additional source apart from riverine and estuarine DOM. This was underlined by higher elemental sulfur-to-carbon ratios in DOM and increased sulfur content of molecular formulae at salinity > 25 (Fig. 7c, 7d). The enrichment of sulfur-containing DOM therefore highlights the influence of tidal flats on the DOM composition in the German Bight.

Moore et al. (2011) estimated that up to 70×10^4 mol DOC is exported from the backbarrier area of Spiekeroog (ca. 73 km²) during each tidal cycle to the North Sea by porewater outwelling. This corresponds to approximately 2.6×10^4 mol DOS per tidal cycle, assuming a content of 3.7% DOS in the porewater (Pohlabein et al. 2017). Thus, the back barrier area of Spiekeroog Island could potentially release around 0.6 mol DOS s⁻¹. Considering the measured DOS concentrations in the Elbe, Weser, and Ems estuaries (2, 2.5, and 3.3 μM DOS, respectively, Supplementary Table S3) and average river discharge values (Elbe 860, Weser 323, and Ems 80 m³ s⁻¹) (Lübben et al. 2009; Schmidt et al. 2011), the estimated DOS exports are approximately 1.7 mol DOS s⁻¹ (Elbe), 0.8 mol DOS s⁻¹ (Weser), and 0.3 mol DOS s⁻¹ (Ems). These estimates are rough and neither consider spatial and seasonal variations in

DOS concentrations nor highly resolved data from the rivers and the Wadden Sea area. However, they suggest that DOS export from the backbarrier tidal flats of Spiekeroog alone is comparable to DOS discharge from the Ems River. Extrapolating the estimates to the entire Wadden Sea intertidal flat area (excluding estuaries), which spans approximately 1688 km² (Grunwald et al. 2010), even yields an export of about 13.7 mol DOS s⁻¹, exceeding the estimated DOS export from the three largest rivers combined (2.8 mol DOS s⁻¹). Although further measurements are certainly needed to validate these estimates, they indicate that intertidal flats are a significant source of DOS to the North Sea.

Conclusions

Our study identified sources and sinks contributing to the distribution of DOM, trace metals, and nutrients in the German Bight. The DOM composition in the German Bight was influenced by a combination of riverine inputs, marine (autochthonous) sources, and porewater outwelling. Molecular-level changes were related to a shift from riverine aromatic, terrestrial signatures nearshore to more aliphatic, nitrogen-containing marine DOM offshore. Porewater outwelling from intertidal flats was identified as an additional source for DOS, most trace metals, and nutrients (DIP, DSi). Negative deviations of DSi from conservative mixing suggested removal by diatoms at the onset of the spring phytoplankton bloom. Trace metals, especially Gd, Ba, Co, and W, showed positive deviations from conservative mixing and highest concentrations at low tide during tidal cycle sampling demonstrating that porewater outwelling from tidal flats is an additional important source besides rivers.

Aromatic DOM and DBC mainly originated from riverine sources, with porewater outwelling as additional DBC source to the water column. However, we found no indications of DBC enrichments in the southern North Sea. This suggests a balance between removal of riverine DBC, for example by photo-degradation and flocculation, and replenishment by porewater-derived DBC. Input of sulfur-enriched DOM was related to rivers. However, in line with the non-conservative mixing of trace metals, elevated sulfur-to-carbon ratios in the intertidal Wadden Sea area, along with elevated SPE-DOS concentrations during

low tide in our tidal cycle sampling, revealed porewater outwelling from tidal flats as an important source. These findings demonstrate that tidal flats are important sources for potentially recalcitrant DOS.

Via the application of DOM molecular indexes as tracers for terrestrial and porewater-derived DOM (I_{TERR} , I_{SUP}), we showed that estuaries and intertidal flats are major sources of DOM to the German Bight and that this DOM is probably recalcitrant on the time scales of nearshore mixing. Our study confirms that intertidal flats have an important effect on elemental budgets in the German Bight and they may be similarly important in other coastal ecosystems. The application of molecular DOM proxies (e.g., I_{TERR} , I_{SUP}), in combination with trace metal data, provides a powerful approach to differentiate the relative contributions of different DOM sources in highly complex coastal ecosystems. Future analytical approaches should include studying the variability of riverine and porewater endmembers, as well as better resolved estuarine transects, ideally in combination with chromophoric DOM measurements, which can be routinely achieved with optical sensors of ferry boxes and at time series stations.

Acknowledgements We thank the captain, crew, and chief scientist Thomas Badewien of *R/V Heincke* (HE527). We also thank Ina Ulber, Matthias Friebe, Melina Knoke, Katrin Klaproth, Jutta Niggemann, Heike Simon, Eleonore Gründken, and Carola Lehnert (ICBM, Oldenburg) for their analytical and scientific support. Anne Köhler (IOW) is thanked for supporting ICP-OES/MS analytics. We also thank Corinna Mori (ICBM, Oldenburg) for valuable comments and suggestions on an earlier version of the manuscript. We appreciate the constructive comments of the anonymous reviewers and the editor, which substantially improved the manuscript. Additional thanks go to the Helmholtz-Zentrum Hereon for providing the FerryBox for this cruise.

Author contributions MS and TD conceived the study; LS, RCS, JW, MB, OD performed chemical analyses and provided data. All authors contributed to data interpretation; RCS, LS, MS wrote the manuscript with significant contributions from all authors.

Funding Open Access funding enabled and organized by Projekt DEAL. This work was supported by Deutsche Forschungsgemeinschaft (DFG) through the marDOS Project (DI 842/6–1) and within the Cluster of Excellence EXC 2077 “The Ocean Floor – Earth’s Uncharted Interface” (Project number 390741603). RCS received a PhD scholarship funded by the Brazilian Ministry of Education agency (Coordenação de Aperfeiçoamento de Pessoal de Nível Superior, CAPES).

Data availability Data used to produce the results of this manuscript are in the Supplementary Material.

Declarations

Competing interest The authors have not disclosed any competing interests.

Open Access This article is licensed under a Creative Commons Attribution 4.0 International License, which permits use, sharing, adaptation, distribution and reproduction in any medium or format, as long as you give appropriate credit to the original author(s) and the source, provide a link to the Creative Commons licence, and indicate if changes were made. The images or other third party material in this article are included in the article's Creative Commons licence, unless indicated otherwise in a credit line to the material. If material is not included in the article's Creative Commons licence and your intended use is not permitted by statutory regulation or exceeds the permitted use, you will need to obtain permission directly from the copyright holder. To view a copy of this licence, visit <http://creativecommons.org/licenses/by/4.0/>.

References

- Abdulla HAN, Minor EC, Dias RF, Hatcher PG (2013) Transformations of the chemical compositions of high molecular weight DOM along a salinity transect: using two dimensional correlation spectroscopy and principal component analysis approaches. *Geochim Cosmochim Acta* 118:231–246. <https://doi.org/10.1016/j.gca.2013.03.036>
- Abril G, Frankignoulle M (2001) Nitrogen–alkalinity interactions in the highly polluted scheldt basin (belgium). *Water Res* 35:844–850. [https://doi.org/10.1016/S0043-1354\(00\)00310-9](https://doi.org/10.1016/S0043-1354(00)00310-9)
- Anderson TF, Pratt LM (1995) Isotopic evidence for the origin of organic sulfur and elemental sulfur in marine sediments, pp 378–396. <https://doi.org/10.1021/bk-1995-0612.ch021>
- Arar EJ, Collins GB (1997) Method 445.0: chlorophyll A. U.S. Environ. Prot. Agency 1–22
- Bao H, Niggemann J, Luo L, Dittmar T, Kao SJ (2017) Aerosols as a source of dissolved black carbon to the ocean. *Nat Commun*. <https://doi.org/10.1038/s41467-017-00437-3>
- Beck M, Brumsack HJ (2012) Biogeochemical cycles in sediment and water column of the Wadden Sea: the example Spiekeroog Island in a regional context. *Ocean Coast Manag* 68:102–113. <https://doi.org/10.1016/j.ocecoaman.2012.05.026>
- Beck M, Dellwig O, Holstein JM, Grunwald M, Liebezeit G, Schnetger B, Brumsack HJ (2008a) Sulphate, dissolved organic carbon, nutrients and terminal metabolic products in deep pore waters of an intertidal flat. *Biogeochemistry* 89:221–238. <https://doi.org/10.1007/s10533-008-9215-6>
- Beck M, Dellwig O, Schnetger B, Brumsack HJ (2008b) Cycling of trace metals (Mn, Fe, Mo, U, V, Cr) in deep pore waters of intertidal flat sediments. *Geochim Cosmochim Acta* 72:2822–2840. <https://doi.org/10.1016/j.gca.2008.04.013>
- Beck M, Dellwig O, Fischer S, Schnetger B, Brumsack H-J (2012) Trace metal geochemistry of organic carbon-rich watercourses draining the NW German coast. *Estuar Coast Shelf Sci* 104–105:66–79. <https://doi.org/10.1016/j.ecss.2012.03.025>
- Beck M, Reckhardt A, Amelsberg J, Bartholomä A, Brumsack HJ, Cypionka H, Dittmar T, Engelen B, Greskowiak J, Hillebrand H, Holtappels M, Neuholz R, Köster J, Kuypers MMM, Massmann G, Meier D, Niggemann J, Paffrath R, Pahnke K, Rovo S, Striebel M, Vandieken V, Wehrmann A, Zielinski O (2017) The drivers of biogeochemistry in beach ecosystems: a cross-shore transect from the dunes to the low-water line. *Mar Chem* 190:35–50. <https://doi.org/10.1016/j.marchem.2017.01.001>
- Beck M, Dellwig O, Schnetger B, Riedel T, Brumsack HJ (2020) Manganese dynamics in tidal basins of the Wadden Sea: spatial/seasonal patterns and budget estimates. *Mar Chem* 225:103847. <https://doi.org/10.1016/j.marchem.2020.103847>
- Becker GA, Dick S, Dippner JW (1992) Hydrography of the German Bight. *Mar Ecol Prog Ser* 91:9–18. <https://doi.org/10.3354/meps091009>
- Berrang PG, Grill EV (1974) The effect of manganese oxide scavenging on molybdenum in saanich inlet, British Columbia. *Mar Chem* 2:125–148. [https://doi.org/10.1016/0304-4203\(74\)90033-4](https://doi.org/10.1016/0304-4203(74)90033-4)
- Beusen AHW, Bouwman AF, Dürr HH, Dekkers ALM, Hartmann J (2009) Global patterns of dissolved silica export to the coastal zone: Results from a spatially explicit global model. *Global Biogeochem Cycles*. <https://doi.org/10.1029/2008GB003281>
- Brockmann U, Topcu D, Schütt M, Leujak W (2018) Eutrophication assessment in the transit area German Bight (North Sea) 2006–2014—stagnation and limitations. *Mar Pollut Bull* 136:68–78. <https://doi.org/10.1016/j.marpolbul.2018.08.060>
- Brodowski S, Rodionov A, Haumaier L, Glaser B, Amelung W (2005) Revised black carbon assessment using benzene polycarboxylic acids. *Org Geochem* 36:1299–1310
- Bruland KW, Lohan MC (2003) Controls of trace metals in seawater. In: *Treatise on geochemistry*. Elsevier, pp. 23–47. <https://doi.org/10.1016/B0-08-043751-6/06105-3>
- Brünjes J, Seidel M, Dittmar T, Niggemann J, Schubotz F (2022) Natural asphalt seeps are potential sources for recalcitrant oceanic dissolved organic sulfur and dissolved black carbon. *Environ Sci Technol*. <https://doi.org/10.1021/acs.est.2c01123>
- Burdige DJ (1993) The biogeochemistry of manganese and iron reduction in marine sediments. *Earth Sci Rev* 35:249–284. [https://doi.org/10.1016/0012-8252\(93\)90040-E](https://doi.org/10.1016/0012-8252(93)90040-E)
- Burdige DJ, Komada T, Magen C, Chanton JP (2016) Modeling studies of dissolved organic matter cycling in Santa Barbara Basin (CA, USA) sediments. *Geochim Cosmochim Acta* 195:100–119. <https://doi.org/10.1016/j.gca.2016.09.007>

- Burnett WC, Bokuniewicz H, Huettel M, Moore WS, Taniguchi M (2003) Groundwater and pore water inputs to the coastal zone. *Biogeochemistry* 66:3–33. <https://doi.org/10.1023/B:BI0G.0000006066.21240.53>
- Byrd JT, Lee KW, Lee DS, Smith RG, Windom HL (1990) The behavior of trace metals in the Geum Estuary, Korea. *Estuaries* 13:8. <https://doi.org/10.2307/1351426>
- Callies U, Gaslikova L, Kapitza H, Scharfe M (2017) German Bight residual current variability on a daily basis: principal components of multi-decadal barotropic simulations. *Geo-Marine Lett* 37:151–162. <https://doi.org/10.1007/s00367-016-0466-2>
- Canuel EA, Cammer SS, McIntosh HA, Pondell CR (2012) Climate change impacts on the organic carbon cycle at the land-ocean interface. *Annu Rev Earth Planet Sci* 40:685–711. <https://doi.org/10.1146/annurev-earth-042711-105511>
- Carey JC, Fulweiler RW (2014) Salt marsh tidal exchange increases residence time of silica in estuaries. *Limnol Oceanogr* 59:1203–1212. <https://doi.org/10.4319/lo.2014.59.4.1203>
- Carlson CA, Hansell DA (2015) DOM sources, sinks, reactivity, and budgets. In: *Biogeochemistry of marine dissolved organic matter*. Elsevier, pp 65–126. <https://doi.org/10.1016/B978-0-12-405940-5.00003-0>
- Carstensen J, Duarte CM (2019) Drivers of pH variability in coastal ecosystems. *Environ Sci Technol* 53:4020–4029. <https://doi.org/10.1021/acs.est.8b03655>
- Chester R, Jickells TD (2012) Marine geochemistry, 3rd edn. In: *Marine geochemistry*. Wiley-Blackwell, Chichester. <https://doi.org/10.1002/9781118349083>
- Coble PG (1996) Characterization of marine and terrestrial DOM in seawater using excitation-emission matrix spectroscopy. *Mar Chem* 51:325–346. [https://doi.org/10.1016/0304-4203\(95\)00062-3](https://doi.org/10.1016/0304-4203(95)00062-3)
- Coffey M, Dehairs F, Collette O, Luther G, Church T, Jickells T (1997) The behaviour of dissolved barium in estuaries. *Estuar Coast Shelf Sci* 45:113–121. <https://doi.org/10.1006/ecss.1996.0157>
- Cole JJ, Lane JM, Marino R, Howarth RW (1993) Molybdenum assimilation by cyanobacteria and phytoplankton in freshwater and salt water. *Limnol Oceanogr* 38:25–35. <https://doi.org/10.4319/lo.1993.38.1.0025>
- Collier RW (1985) Molybdenum in the northeast pacific ocean. *Limnol Oceanogr* 30:1351–1354. <https://doi.org/10.4319/lo.1985.30.6.1351>
- Coppola AI, Druffel ERM (2016) Cycling of black carbon in the ocean. *Geophys Res Lett* 43:4477–4482. <https://doi.org/10.1002/2016GL068574>
- Coppola AI, Wagner S, Lennartz ST, Seidel M, Ward ND, Dittmar T, Santín C, Jones MW (2022) The black carbon cycle and its role in the Earth system. *Nat Rev Earth Environ* 3:516–532. <https://doi.org/10.1038/s43017-022-00316-6>
- Cui M, Luther GW, Gomes M (2021) Cycling of W and Mo species in natural sulfidic waters and their sorption mechanisms on MnO₂ and implications for paired W and Mo records as a redox proxy. *Geochim Cosmochim Acta* 295:24–48. <https://doi.org/10.1016/j.gca.2020.12.007>
- Dai M, Guo X, Zhai W, Yuan L, Wang B, Wang L, Cai P, Tang T, Cai W-J (2006) Oxygen depletion in the upper reach of the Pearl River estuary during a winter drought. *Mar Chem* 102:159–169. <https://doi.org/10.1016/j.marchem.2005.09.020>
- Dellwig O, Beck M, Lemke A, Lunau M, Kolditz K, Schnetger B, Brumsack H-J (2007a) Non-conservative behaviour of molybdenum in coastal waters: coupling geochemical, biological, and sedimentological processes. *Geochim Cosmochim Acta* 71:2745–2761. <https://doi.org/10.1016/j.gca.2007.03.014>
- Dellwig O, Bosselmann K, Kölsch S, Hentscher M, Hinrichs J, Böttcher ME, Reuter R, Brumsack H-J (2007b) Sources and fate of manganese in a tidal basin of the German Wadden Sea. *J Sea Res* 57:1–18. <https://doi.org/10.1016/j.seares.2006.1007.1006>
- Dellwig O, Wegwerth A, Schnetger B, Schulz H, Arz HW (2019) Dissimilar behaviors of the geochemical twins W and Mo in hypoxic-euxinic marine basins. *Earth-Sci Rev* 193:1–23. <https://doi.org/10.1016/j.earscirev.2019.03.017>
- Dellwig O, Wegwerth A, Arz HW (2021) Anatomy of the Major Baltic Inflow in 2014: impact of manganese and iron shuttling on phosphorus and trace metals in the Gotland Basin. *Baltic Sea Cont Shelf Res* 223:104449. <https://doi.org/10.1016/j.csr.2021.104449>
- Dittmar T (2008) The molecular level determination of black carbon in marine dissolved organic matter. *Org Geochem* 39:396–407. <https://doi.org/10.1016/j.orggeochem.2008.01.015>
- Dittmar T, Paeng J (2009) A heat-induced molecular signature in marine dissolved organic matter. *Nat Geosci* 2:175–179. <https://doi.org/10.1038/ngeo440>
- Dittmar T, Stubbins A (2014) Dissolved organic matter in aquatic systems. In: *Treatise on geochemistry*. Elsevier, pp 125–156. <https://doi.org/10.1016/B978-0-08-095975-7.01010-X>
- Domingues RB, Barbosa AB, Sommer U, Galvão HM (2011) Ammonium, nitrate and phytoplankton interactions in a freshwater tidal estuarine zone: potential effects of cultural eutrophication. *Aquat Sci* 73:331–343. <https://doi.org/10.1007/s00027-011-0180-0>
- Ebeling A, Zimmermann T, Klein O, Irrgeher J, Pröfrock D (2022) Analysis of seventeen certified water reference materials for trace and technology-critical elements. *Geostand Geoanalytical Res* 46:351–378. <https://doi.org/10.1111/ggr.12422>
- Ehlert von Ahn CM, Böttcher ME, Malik C, Westphal J, Rach B, Nantke CKM, Jenner A-K, Saban R, Winde V, Schmiedinger I (2023) Spatial and temporal variations in the isotope hydrobiogeochemistry of a managed river draining towards the southern Baltic Sea. *Geochemistry*. <https://doi.org/10.1016/j.chemer.2023.125979>
- Firdaus M, Norisuye K, Nakagawa Y, Nakatsuka S, Sohrin Y (2008) Dissolved and labile particulate Zr, Hf, Nb, Ta, Mo and W in the western North Pacific Ocean. *J Oceanogr* 64:247–257. <https://doi.org/10.1007/s10872-008-0019-z>
- Flerus R, Lechtenfeld OJ, Koch BP, McCallister SL, Schmitt-Kopplin P, Benner R, Kaiser K, Kattner G (2012) A molecular perspective on the ageing of marine dissolved

- organic matter. *Biogeosciences* 9:1935–1955. <https://doi.org/10.5194/bg-9-1935-2012>
- Francescangeli F, Milker Y, Bunzel D, Thomas H, Norbisch-rath M, Schönfeld J, Schmiedl G (2021) Recent benthic foraminiferal distribution in the Elbe Estuary (North Sea, Germany): a response to environmental stressors. *Estuar Coast Shelf Sci* 251:107198. <https://doi.org/10.1016/j.ecss.2021.107198>
- Gomez-Saez GV, Pohlabein AM, Stubbins A, Marsay CM, Dittmar T (2017) Photochemical alteration of dissolved organic sulfur from sulfidic porewater. *Environ Sci Technol* 51:14144–14154. <https://doi.org/10.1021/acs.est.7b03713>
- Gonneea ME, Mulligan AE, Charette MA (2013) Seasonal cycles in radium and barium within a subterranean estuary: Implications for groundwater derived chemical fluxes to surface waters. *Geochim Cosmochim Acta* 119:164–177
- Gonsior M, Peake BM, Cooper WT, Podgorski DC, D'Andrilli J, Dittmar T, Cooper WJ (2011) Characterization of dissolved organic matter across the Subtropical Convergence off the South Island, New Zealand. *Mar Chem* 123:99–110. <https://doi.org/10.1016/j.marchem.2010.10.004>
- Grunwald M, Dellwig O, Beck M, Dippner JW, Freund JA, Kohlmeier C, Schnetger B, Brumsack HJ (2009) Methane in the southern North Sea: sources, spatial distribution and budgets. *Estuar Coast Shelf Sci* 81:445–456. <https://doi.org/10.1016/j.ecss.2008.11.021>
- Grunwald M, Dellwig O, Kohlmeier C, Kowalski N, Beck M, Badewien TH, Kotzur S, Liebezeit G, Brumsack H-JJ (2010) Nutrient dynamics in a back barrier tidal basin of the Southern North Sea: time-series, model simulations, and budget estimates. *J Sea Res* 64:199–212. <https://doi.org/10.1016/j.seares.2010.02.008>
- Hansell DA (2013) Recalcitrant dissolved organic carbon fractions. *Ann Rev Mar Sci* 5:421–445. <https://doi.org/10.1146/annurev-marine-120710-100757>
- Hansman RL, Dittmar T, Herndl GJ (2015) Conservation of dissolved organic matter molecular composition during mixing of the deep water masses of the northeast Atlantic Ocean. *Mar Chem* 177:288–297. <https://doi.org/10.1016/j.marchem.2015.06.001>
- Hatje V, Bruland KW, Flegal AR (2016) Increases in anthropogenic gadolinium anomalies and rare earth element concentrations in San Francisco Bay over a 20 year record. *Environ Sci Technol* 50:4159–4168. <https://doi.org/10.1021/acs.est.5b04322>
- Hofmann J, Behrendt H, Gilbert A, Janssen R, Kannen A, Kappenberg J, Lenhart H, Lise W, Nunneri C, Windhorst W (2005) Catchment–coastal zone interaction based upon scenario and model analysis: Elbe and the German Bight case study. *Reg Environ Chang* 5:54–81. <https://doi.org/10.1007/s10113-004-0082-y>
- Houben GJ, Post VEA, Gröger-Trampe J, Pesci MH, Sültenfuß J (2021) On the propagation of reaction fronts in a sandy aquifer over 20+ years: lessons from a test site in North-western Germany. *Water Resour Res*. <https://doi.org/10.1029/2020WR028706>
- Howarth RW (1998) An assessment of human influences on fluxes of nitrogen from the terrestrial landscape to the estuaries and continental shelves of the North Atlantic Ocean. *Nutr Cycl Agroecosystems* 52:213–223. <https://doi.org/10.1023/a:1009784210657>
- Jaffé R, Ding Y, Niggemann J, Vähätalo AV, Stubbins A, Spencer RGM, Campbell J, Dittmar T (2013) Global charcoal mobilization from soils via dissolution and riverine transport to the oceans. *Science* 340:345–347. <https://doi.org/10.1126/science.1231476>
- Johannesson KH, Palmore CD, Fackrell J, Prouty NG, Swarzenski PW, Chevis DA, Telfeyan K, White CD, Burdige DJ (2017) Rare earth element behavior during groundwater–seawater mixing along the Kona Coast of Hawaii. *Geochim Cosmochim Acta* 198:229–258. <https://doi.org/10.1016/j.gca.2016.11.009>
- Kappenberg A, Bläsing M, Lehndorff E, Amelung W (2016) Black carbon assessment using benzene polycarboxylic acids: limitations for organic-rich matrices. *Org Geochem* 94:47–51. <https://doi.org/10.1016/j.orggeochem.2016.01.009>
- Kashiwabara T, Takahashi Y, Marcus MA, Uruga T, Tanida H, Terada Y, Usui A (2013) Tungsten species in natural ferromanganese oxides related to its different behavior from molybdenum in oxic ocean. *Geochim Cosmochim Acta* 106:364–378. <https://doi.org/10.1016/j.gca.2012.12.026>
- Kashiwabara T, Kubo S, Tanaka M, Senda R, Iizuka T, Tanimizu M, Takahashi Y (2017) Stable isotope fractionation of tungsten during adsorption on Fe and Mn (oxyhydr) oxides. *Geochim Cosmochim Acta* 204:52–67. <https://doi.org/10.1016/j.gca.2017.01.031>
- Knoke M, Dittmar T, Zielinski O, Kida M, Asp NE, De Rezende CE, Schnetger B, Seidel M (2024) Outwelling of reduced porewater drives the biogeochemistry of dissolved organic matter and trace metals in a major mangrove-fringed estuary in Amazonia. *Limnol Oceanogr*. <https://doi.org/10.1002/lno.12473>
- Koch BP, Dittmar T (2006) From mass to structure: an aromaticity index for high-resolution mass data of natural organic matter. *Rapid Commun Mass Spectrom* 20:926–932. <https://doi.org/10.1002/rcm.2386>
- Koch BP, Dittmar T (2016) From mass to structure: an aromaticity index for high-resolution mass data of natural organic matter. *Rapid Commun Mass Spectrom* 30:250–250. <https://doi.org/10.1002/rcm.7433>
- Koch BP, Witt M, Engbrodt R, Dittmar T, Kattner G (2005) Molecular formulae of marine and terrigenous dissolved organic matter detected by electrospray ionization Fourier transform ion cyclotron resonance mass spectrometry. *Geochim Cosmochim Acta* 69:3299–3308. <https://doi.org/10.1016/j.gca.2005.02.027>
- Kowalski N, Dellwig O, Beck M, Grunwald M, Fischer S, Piepho M, Riedel T, Freund H, Brumsack HJ, Böttcher ME (2009) Trace metal dynamics in the water column and pore waters in a temperate tidal system: response to the fate of algae-derived organic matter. *Ocean Dyn* 59:333–350. <https://doi.org/10.1007/s10236-009-0192-7>
- Kowalski N, Dellwig O, Beck M, Grunwald M, Dürselen C-D, Badewien TH, Brumsack H-J, van Beusekom JEE, Böttcher ME (2012) A comparative study of manganese dynamics in the water column and sediments of intertidal systems of the North Sea. *Estuar Coast Shelf Sci* 100:3–17. <https://doi.org/10.1016/j.ecss.2011.03.011>

- Kowalski N, Dellwig O, Beck M, Gräwe U, Neubert N, Nägler TF, Badewien TH, Brumsack H-J, van Beusekom JEE, Böttcher ME (2013) Pelagic molybdenum concentration anomalies and the impact of sediment resuspension on the molybdenum budget in two tidal systems of the North Sea. *Geochim Cosmochim Acta* 119:198–211. <https://doi.org/10.1016/j.gca.2013.05.046>
- Ksionzek KB, Lechtenfeld OJ, McCallister SL, Schmitt-Kopplin P, Geuer JK, Geibert W, Koch BP (2016) Dissolved organic sulfur in the ocean: Biogeochemistry of a petagram inventory. *Science* 354:456–459. <https://doi.org/10.1126/science.aaf7796>
- Kulaksiz S, Bau M (2007) Contrasting behaviour of anthropogenic gadolinium and natural rare earth elements in estuaries and the gadolinium input into the North Sea. *Earth Planet Sci Lett* 260:361–371. <https://doi.org/10.1016/j.epsl.2007.06.016>
- Laperriere SM, Nidzicko NJ, Fox RJ, Fisher AW, Santoro AE (2019) Observations of variable ammonia oxidation and nitrous oxide flux in a eutrophic estuary. *Estuar Coasts* 42:33–44. <https://doi.org/10.1007/s12237-018-0441-4>
- Laxen DPH, Davison W, Woof C (1984) Manganese chemistry in rivers and streams. *Geochim Cosmochim Acta* 48:2107–2111. [https://doi.org/10.1016/0016-7037\(84\)90390-9](https://doi.org/10.1016/0016-7037(84)90390-9)
- Lechtenfeld OJ, Kattner G, Flerus R, McCallister SL, Schmitt-Kopplin P, Koch BP (2014) Molecular transformation and degradation of refractory dissolved organic matter in the Atlantic and Southern Ocean. *Geochim Cosmochim Acta* 126:321–337. <https://doi.org/10.1016/j.gca.2013.11.009>
- Letourneau ML, Schaefer SC, Chen H, McKenna AM, Alber M, Medeiros PM (2021) Spatio-temporal changes in dissolved organic matter composition along the salinity gradient of a marsh-influenced estuarine complex. *Limnol Oceanogr* 66:3040–3054. <https://doi.org/10.1002/lno.11857>
- Linkhorst A, Dittmar T, Waska H (2017) Molecular fractionation of dissolved organic matter in a shallow Subterranean Estuary: the role of the iron curtain. *Environ Sci Technol* 51:1312–1320. <https://doi.org/10.1021/acs.est.6b03608>
- Longnecker K, Oswald L, Kido Soule MC, Cutter GA, Kujawinski EB (2020) Organic sulfur: a spatially variable and understudied component of marine organic matter. *Limnol Oceanogr Lett* 5:305–312. <https://doi.org/10.1002/lo2.10149>
- Lübben A, Dellwig O, Koch S, Beck M, Badewien TH, Fischer S, Reuter R (2009) Distributions and characteristics of dissolved organic matter in temperate coastal waters (Southern North Sea). *Ocean Dyn* 59:263–275. <https://doi.org/10.1007/s10236-009-0181-x>
- Marencic H (2009) Quality status report 2009. Wadden Sea Ecosystem No. 25. Qual. Status Rep. 2009. Wadden Sea Ecosyst. No. 25. 597
- Marie L, Pernet-Coudrier B, Waeles M, Gabon M, Riso R (2015) Dynamics and sources of reduced sulfur, humic substances and dissolved organic carbon in a temperate river system affected by agricultural practices. *Sci Total Environ* 537:23–32. <https://doi.org/10.1016/j.scitotenv.2015.07.089>
- Medeiros PM, Seidel M, Powers LC, Dittmar T, Hansell DA, Miller WL (2015a) Dissolved organic matter composition and photochemical transformations in the northern North Pacific Ocean. *Geophys Res Lett* 42:863–870. <https://doi.org/10.1002/2014GL062663>
- Medeiros PM, Seidel M, Ward ND, Carpenter EJ, Gomes HR, Niggemann J, Krusche AV, Richey JE, Yager PL, Dittmar T (2015b) Fate of the Amazon River dissolved organic matter in the tropical Atlantic Ocean. *Global Biogeochem Cycles* 29:677–690. <https://doi.org/10.1002/2015GB005115>
- Medeiros PM, Seidel M, Niggemann J, Spencer RGM, Hernes PJ, Yager PL, Miller WL, Dittmar T, Hansell DA (2016) A novel molecular approach for tracing terrigenous dissolved organic matter into the deep ocean. *Global Biogeochem Cycles* 30:689–699. <https://doi.org/10.1002/2015GB005320>
- Merder J, Freund JA, Feudel U, Hansen CT, Hawkes JA, Jacob B, Klapproth K, Niggemann J, Noriega-Ortega BE, Osterholz H, Rossel PE, Seidel M, Singer G, Stubbins A, Waska H, Dittmar T (2020) ICBM-OCEAN: processing ultrahigh-resolution mass spectrometry data of complex molecular mixtures. *Anal Chem* 92:6832–6838. <https://doi.org/10.1021/acs.analchem.9b05659>
- Miller CA, Peucker-Ehrenbrink B, Walker BD, Marcantonio F (2011) Re-assessing the surface cycling of molybdenum and rhenium. *Geochim Cosmochim Acta* 75:7146–7179. <https://doi.org/10.1016/j.gca.2011.09.005>
- Mohajerin TJ, Helz GR, Johannesson KH (2016) Tungsten-molybdenum fractionation in estuarine environments. *Geochim Cosmochim Acta* 177:105–119. <https://doi.org/10.1016/j.gca.2015.12.030>
- Moore WS (1997) High fluxes of radium and barium from the mouth of the Ganges-Brahmaputra River during low river discharge suggest a large groundwater source. *Earth Planet Sci Lett* 150:141–150. [https://doi.org/10.1016/S0012-821X\(97\)00083-6](https://doi.org/10.1016/S0012-821X(97)00083-6)
- Moore WS, Blanton JO, Joye SB (2006) Estimates of flushing times, submarine groundwater discharge, and nutrient fluxes to Okatee Estuary, South Carolina. *J Geophys Res Ocean* 111:1–14. <https://doi.org/10.1029/2005JC003041>
- Moore WS, Beck M, Riedel T, Rutgers van der Loeff M, Dellwig O, Shaw TJ, Schnetger B, Brumsack H-J (2011) Radium-based pore water fluxes of silica, alkalinity, manganese, DOC, and uranium: a decade of studies in the German Wadden Sea. *Geochim Cosmochim Acta* 75:6535–6555. <https://doi.org/10.1016/j.gca.2011.08.037>
- Morford JL, Martin WR, Kalnejais LH, François R, Bothner M, Karle IM (2007) Insights on geochemical cycling of U, Re and Mo from seasonal sampling in Boston Harbor, Massachusetts, USA. *Geochim Cosmochim Acta* 71:895–917. <https://doi.org/10.1016/j.gca.2006.10.016>
- Mori C, Santos IR, Brumsack HJ, Schnetger B, Dittmar T, Seidel M (2019) Non-conservative behavior of dissolved organic matter and trace metals (Mn, Fe, Ba) driven by porewater exchange in a subtropical mangrove-estuary. *Front Mar Sci* 6:1–21. <https://doi.org/10.3389/fmars.2019.00481>
- Mori C, Beck M, Striebel M, Merder J, Schnetger B, Dittmar T, Pahnke K, Brumsack H-J (2021) Biogeochemical cycling of molybdenum and thallium during a

- phytoplankton summer bloom: a mesocosm study. *Mar Chem* 229:103910. <https://doi.org/10.1016/j.marchem.2020.103910>
- Morris AW (1975) Dissolved molybdenum and vanadium in the northeast Atlantic Ocean. *Deep Sea Res Oceanogr Abstr* 22:49–54. [https://doi.org/10.1016/0011-7471\(75\)90018-2](https://doi.org/10.1016/0011-7471(75)90018-2)
- Nance WB, Taylor SR (1976) Rare earth element patterns and crustal evolution—I. Australian post-Archean sedimentary rocks. *Geochim Cosmochim Acta* 40:1539–1551. [https://doi.org/10.1016/0016-7037\(76\)90093-4](https://doi.org/10.1016/0016-7037(76)90093-4)
- Nebbioso A, Piccolo A (2013) Molecular characterization of dissolved organic matter (DOM): a critical review. *Anal Bioanal Chem* 405:109–124. <https://doi.org/10.1007/s00216-012-6363-2>
- Nezlin NP, Kamer K, Hyde J, Stein ED (2009) Dissolved oxygen dynamics in a eutrophic estuary, Upper Newport Bay. *California Estuar Coast Shelf Sci* 82:139–151. <https://doi.org/10.1016/j.ecss.2009.01.004>
- Oehler T, Tamborski J, Rahman S, Moosdorf N, Ahrens J, Mori C, Neuholz R, Schnetger B, Beck M (2019) DSI as a tracer for submarine groundwater discharge. *Front Mar Sci* 6:1–13. <https://doi.org/10.3389/fmars.2019.00563>
- Oksanen AJ, Blanchet FG, Friendly M, Kindt R, Legendre P, Mcglinn D, Minchin PR, Hara RBO, Simpson GL, Solyomos P, Stevens MHH, Szocs E (2022) Vegan: community ecology package. R package version 2.6-4. <http://CRAN.R-project.org/package=vegan>
- OSPAR (2000) Quality status report 2000. Region II - Greater North Sea. OSPAR Comm, London, p 11
- Osterholz H, Kirchman DL, Niggemann J, Dittmar T (2016) Environmental drivers of dissolved organic matter molecular composition in the Delaware estuary. *Front Earth Sci*. <https://doi.org/10.3389/feart.2016.00095>
- Paffrath R, Pahnke K, Behrens MK, Reckhardt A, Ehlert C, Schnetger B, Brumsack HJ (2020) Rare earth element behavior in a sandy subterranean estuary of the Southern North Sea. *Front Mar Sci*. <https://doi.org/10.3389/fmars.2020.00424>
- Painter SC, Lapworth DJ, Woodward EMS, Kroeger S, Evans CD, Mayor DJ, Sanders RJ (2018) Terrestrial dissolved organic matter distribution in the North Sea. *Sci Total Environ* 630:630–647. <https://doi.org/10.1016/j.scitotenv.2018.02.237>
- Pedreira RMA, Pahnke K, Böning P, Hatje V (2018) Tracking hospital effluent-derived gadolinium in Atlantic coastal waters off Brazil. *Water Res* 145:62–72. <https://doi.org/10.1016/j.watres.2018.08.005>
- Petersen W, Petschatnikov M, Schroeder F, Colijn F (2003) FerryBox systems for monitoring coastal waters. *Elsevier Oceanogr Ser* 69:325–333. [https://doi.org/10.1016/S0422-9894\(03\)80052-1](https://doi.org/10.1016/S0422-9894(03)80052-1)
- Phillips AA, White ME, Seidel M, Wu F, Pavia FF, Kemeny PC, Ma AC, Aluwihare LI, Dittmar T, Sessions AL (2022) Novel sulfur isotope analyses constrain sulfurized porewater fluxes as a minor component of marine dissolved organic matter. *Proc Natl Acad Sci*. <https://doi.org/10.1073/pnas.2209152119>
- Podgorski DC, Zito P, Kellerman AM, Bekins BA, Cozzarelli IM, Smith DF, Cao X, Schmidt-Rohr K, Wagner S, Stubbins A, Spencer RGM (2021) Hydrocarbons to carboxyl-rich alicyclic molecules: a continuum model to describe biodegradation of petroleum-derived dissolved organic matter in contaminated groundwater plumes. *J Hazard Mater* 402:123998
- Pohlabein AM, Gomez-Saez GV, Noriega-Ortega BE, Dittmar T (2017) Experimental evidence for abiotic sulfurization of marine dissolved organic matter. *Front Mar Sci* 4:1–11. <https://doi.org/10.3389/fmars.2017.00364>
- R Core Team (2022) A language and environment for statistical computing R Foundation for Statistical Computing, Vienna, Austria. <https://www.R-project.org/>
- Reckhardt A, Beck M, Seidel M, Riedel T, Wehrmann A, Bartholomä A, Schnetger B, Dittmar T, Brumsack H-J (2015) Carbon, nutrient and trace metal cycling in sandy sediments: a comparison of high-energy beaches and backbarrier tidal flats. *Estuar Coast Shelf Sci* 159:1–14. <https://doi.org/10.1016/j.ecss.2015.03.025>
- Rehder G, Keir RS, Suess E, Pohlmann T (1998) The multiple sources and patterns of methane in North Sea waters, aquatic geochemistry
- Riedel T, Lettmann K, Schnetger B, Beck M, Brumsack H-J (2011) Rates of trace metal and nutrient diagenesis in an intertidal creek bank. *Geochim Cosmochim Acta* 75:134–147. <https://doi.org/10.1016/j.gca.2010.09.040>
- Riedel T, Zak D, Biester H, Dittmar T (2013) Iron traps terrestrially derived dissolved organic matter at redox interfaces. *Proc Natl Acad Sci* 110:10101–10105. <https://doi.org/10.1073/pnas.1221487110>
- Riedel T, Zark M, Vähätalo AV, Niggemann J, Spencer RGM, Hernes PJ, Dittmar T (2016) Molecular signatures of biogeochemical transformations in dissolved organic matter from ten world rivers. *Front Earth Sci* 4:1–16. <https://doi.org/10.3389/feart.2016.00085>
- Rogowska J, Olkowska E, Ratajczyk W, Wolska L (2018) Gadolinium as a new emerging contaminant of aquatic environments. *Environ Toxicol Chem* 37:1523–1534. <https://doi.org/10.1002/etc.4116>
- Saito MA, Moffett JW (2002) Temporal and spatial variability of cobalt in the Atlantic Ocean. *Geochim Cosmochim Acta* 66:1943–1953. [https://doi.org/10.1016/S0016-7037\(02\)00829-3](https://doi.org/10.1016/S0016-7037(02)00829-3)
- Saito MA, Moffett JW, Chisholm SW, Waterbury JB (2002) Cobalt limitation and uptake in *Prochlorococcus*. *Limnol Oceanogr* 47:1629–1636. <https://doi.org/10.4319/lo.2002.47.6.1629>
- Samanta S, Dalai TK (2016) Dissolved and particulate Barium in the Ganga (Hooghly) River estuary, India: solute-particle interactions and the enhanced dissolved flux to the oceans. *Geochim Cosmochim Acta* 195:1–28. <https://doi.org/10.1016/j.gca.2016.09.005>
- Sanders T, Laanbroek HJ (2018) The distribution of sediment and water column nitrification potential in the hyperturbid Ems estuary. *Aquat Sci* 80:33. <https://doi.org/10.1007/s00027-018-0584-1>
- Santos IRS, Burnett WC, Chanton J, Mwashote B, Suryaputra IGNA, Dittmar T (2008) Nutrient biogeochemistry in a Gulf of Mexico subterranean estuary and groundwater-derived fluxes to the coastal ocean. *Limnol Oceanogr* 53:705–718. <https://doi.org/10.4319/lo.2008.53.2.0705>

- Santos IR, Beck M, Brumsack HJ, Maher DT, Dittmar T, Waska H, Schnetger B (2015) Porewater exchange as a driver of carbon dynamics across a terrestrial-marine transect: insights from coupled ^{222}Rn and pCO_2 observations in the German Wadden Sea. *Mar Chem* 171:10–20. <https://doi.org/10.1016/j.marchem.2015.02.005>
- Santos IR, Burdige DJ, Jennerjahn TC, Bouillon S, Cabral A, Serrano O, Wernberg T, Filbee-Dexter K, Guimond JA, Tamborski JJ (2021a) The renaissance of Odum's outwelling hypothesis in "Blue Carbon" science. *Estuar Coast Shelf Sci* 255:107361. <https://doi.org/10.1016/j.ecss.2021.107361>
- Santos IR, Chen X, Lecher AL, Sawyer AH, Moosdorf N, Rodellas V, Tamborski J, Cho H-M, Dimova N, Sugimoto R, Bonaglia S, Li H, Hajati M-C, Li L (2021b) Submarine groundwater discharge impacts on coastal nutrient biogeochemistry. *Nat Rev Earth Environ* 2:307–323. <https://doi.org/10.1038/s43017-021-00152-0>
- Schlitzer R (2022) Ocean data view. <https://odv.awi.de>
- Schmidt F, Elvert M, Koch BP, Witt M, Hinrichs KU (2009) Molecular characterization of dissolved organic matter in pore water of continental shelf sediments. *Geochim Cosmochim Acta* 73:3337–3358. <https://doi.org/10.1016/j.gca.2009.03.008>
- Schmidt C, Hanfland C, Regnier P, Van Cappellen P, Schlüter M, Knauth U, Stimac I, Geibert W (2011) ^{228}Ra , ^{226}Ra , ^{224}Ra and ^{223}Ra in potential sources and sinks of land-derived material in the German Bight of the North Sea: implications for the use of radium as a tracer. *Geo-Marine Lett* 31:259–269. <https://doi.org/10.1007/s00367-011-0231-5>
- Schnetger B, Lehnrs C (2014) Determination of nitrate plus nitrite in small volume marine water samples using vanadium(III)chloride as a reduction agent. *Mar Chem* 160:91–98. <https://doi.org/10.1016/j.marchem.2014.01.010>
- Seidel M, Beck M, Riedel T, Waska H, Suryaputra IGNA, Schnetger B, Niggemann J, Simon M, Dittmar T (2014) Biogeochemistry of dissolved organic matter in an anoxic intertidal creek bank. *Geochim Cosmochim Acta* 140:418–434. <https://doi.org/10.1016/j.gca.2014.05.038>
- Seidel M, Beck M, Greskowiak J, Riedel T, Waska H, Suryaputra IGNA, Schnetger B, Niggemann J, Simon M, Dittmar T (2015a) Benthic-pelagic coupling of nutrients and dissolved organic matter composition in an intertidal sandy beach. *Mar Chem* 176:150–163. <https://doi.org/10.1016/j.marchem.2015.08.011>
- Seidel M, Yager PL, Ward ND, Carpenter EJ, Gomes HR, Krusche AV, Richey JE, Dittmar T, Medeiros PM (2015b) Molecular-level changes of dissolved organic matter along the Amazon River-to-ocean continuum. *Mar Chem* 177:218–231. <https://doi.org/10.1016/j.marchem.2015.06.019>
- Seidel M, Manecki M, Herlemann DPR, Deutsch B, Schulz-Bull D, Jürgens K, Dittmar T (2017) Composition and transformation of dissolved organic matter in the Baltic sea. *Front Earth Sci* 5:1–20. <https://doi.org/10.3389/feart.2017.00031>
- Sleighter RL, Hatcher PG (2008) Molecular characterization of dissolved organic matter (DOM) along a river to ocean transect of the lower Chesapeake Bay by ultrahigh resolution electrospray ionization Fourier transform ion cyclotron resonance mass spectrometry. *Mar Chem* 110:140–152. <https://doi.org/10.1016/j.marchem.2008.04.008>
- Sloppy CP, Van der Gaast SJ, Van Raaphorst W (1996) Phosphorus binding by poorly crystalline iron oxides in North Sea sediments. *Mar Chem* 52:55–73. [https://doi.org/10.1016/0304-4203\(95\)00078-X](https://doi.org/10.1016/0304-4203(95)00078-X)
- Smedley PL, Kinniburgh DG (2017) Molybdenum in natural waters: a review of occurrence, distributions and controls. *Appl Geochem* 84:387–432. <https://doi.org/10.1016/j.apgeochem.2017.05.008>
- Sohrin Y, Matsui M, Nakayama E (1999) Contrasting behavior of tungsten and molybdenum in the Okinawa Trough, the East China Sea and the Yellow Sea. *Geochim Cosmochim Acta* 63:3457–3466. [https://doi.org/10.1016/S0016-7037\(99\)00273-2](https://doi.org/10.1016/S0016-7037(99)00273-2)
- Stubbins A, Spencer RGM, Chen H, Hatcher PG, Mopper K, Hernes PJ, Mwamba VL, Mangangu AM, Wabakanghanzi JN, Six J (2010) Illuminated darkness: molecular signatures of Congo River dissolved organic matter and its photochemical alteration as revealed by ultrahigh precision mass spectrometry. *Limnol Oceanogr* 55:1467–1477. <https://doi.org/10.4319/lo.2010.55.4.1467>
- Stubbins A, Niggemann J, Dittmar T (2012) Photo-lability of deep ocean dissolved black carbon. *Biogeosciences* 9:1661–1670. <https://doi.org/10.5194/bg-9-1661-2012>
- Sunda WG, Huntsman SA (1995) Cobalt and zinc interreplacement in marine phytoplankton: biological and geochemical implications. *Limnol Oceanogr* 40:1404–1417. <https://doi.org/10.4319/lo.1995.40.8.1404>
- Sundby B, Anderson LG, Hall POJ, Iverfeldt Å, van der Loeff MMR, Westerlund SFG (1986) The effect of oxygen on release and uptake of cobalt, manganese, iron and phosphate at the sediment-water interface. *Geochim Cosmochim Acta* 50:1281–1288. [https://doi.org/10.1016/0016-7037\(86\)90411-4](https://doi.org/10.1016/0016-7037(86)90411-4)
- Tribovillard N, Algeo TJ, Lyons T, Riboulleau A (2006) Trace metals as paleoredox and paleoproductivity proxies: an update. *Chem Geol* 232:12–32. <https://doi.org/10.1016/j.chemgeo.2006.02.012>
- Tzortziou M, Neale PJ, Osburn CL, Megonigal JP, Maie N, Jaffé R (2008) Tidal marshes as a source of optically and chemically distinctive colored dissolved organic matter in the Chesapeake Bay. *Limnol Oceanogr* 53:148–159. <https://doi.org/10.4319/lo.2008.53.1.0148>
- Valle-Levinson A, Stanev E, Badewien TH (2018) Tidal and subtidal exchange flows at an inlet of the Wadden Sea. *Estuar Coast Shelf Sci* 202:270–279. <https://doi.org/10.1016/j.ecss.2018.01.013>
- Vuori KM (1995) Direct and indirect effects of iron on river ecosystems. *Ann Zool Fennici* 32:317–329
- Wagner S, Riedel T, Niggemann J, Vähätalo AV, Dittmar T, Jaffé R (2015) Linking the molecular signature of heteroatomic dissolved organic matter to watershed characteristics in world rivers. *Environ Sci Technol* 49:13798–13806. <https://doi.org/10.1021/acs.est.5b00525>
- Wagner S, Jaffé R, Stubbins A (2018) Dissolved black carbon in aquatic ecosystems. *Limnol Oceanogr Lett* 3:168–185. <https://doi.org/10.1002/lo2.10076>

- Ward ND, Bianchi TS, Medeiros PM, Seidel M, Richey JE, Keil RG, Sawakuchi HO (2017) Where carbon goes when water flows: carbon cycling across the aquatic continuum. *Front Mar Sci* 4:1–27. <https://doi.org/10.3389/fmars.2017.00007>
- Waska H, Greskowiak J, Ahrens J, Beck M, Ahmerkamp S, Böning P, Brumsack HJ, Degenhardt J, Ehlert C, Engelen B, Grünenbaum N, Holtappels M, Pahnke K, Marchant HK, Massmann G, Meier D, Schnetger B, Schwalfenberg K, Simon H, Vandieken V, Zielinski O, Dittmar T (2019) Spatial and temporal patterns of pore water chemistry in the inter-tidal zone of a high energy beach. *Front Mar Sci* 6:1–16. <https://doi.org/10.3389/fmars.2019.00154>
- Winterwerp JC, Vroom J, Wang ZB, Krebs M, Hendriks ECM, van Maren DS, Schrottke K, Borgsmüller C, Schöl A (2017) SPM response to tide and river flow in the hyper-turbid Ems River. *Ocean Dyn* 67:559–583. <https://doi.org/10.1007/s10236-017-1043-6>
- Yamashita Y, Jaffé R, Maie N, Tanoue E (2008) Assessing the dynamics of dissolved organic matter (DOM) in coastal environments by excitation emission matrix fluorescence and parallel factor analysis (EEM-PARAFAC). *Limnol Oceanogr* 53:1900–1908. <https://doi.org/10.4319/lo.2008.53.5.1900>
- Zark M, Dittmar T (2018) Universal molecular structures in natural dissolved organic matter. *Nat Commun* 9:1–8. <https://doi.org/10.1038/s41467-018-05665-9>
- Zeiler M, Schwarzer K, Ricklefs K (2008) Seabed morphology and sediment dynamics. *Küste*, pp 31–44

Publisher's Note Springer Nature remains neutral with regard to jurisdictional claims in published maps and institutional affiliations.